J Nanostruct 16(4): 5027-5053, Autumn 2026

RESEARCH PAPER

Cinnamon (Cinnamomum verum) Mediated Silver Nanoparticles as Green Corrosion Inhibitors for C45 Steel in Hydrochloric Acid

Ayat J. Kadhim [1], Ahmed S. Shanta Alsadkhan [2], Ghufran A. Mohammed [1], A M Jabbar [3], Ayat N. Hassan [4], Noor H. Faisal [4], Raneen S. Swadi [4], Zahraa M Khalid [1], Zahraa M Hammoud [1], Zaidon T. Al aqbi [1]*

[1] *Department of Chemistry, College of Science, University of Misan, Misan, Iraq.*

[2] *Department of Medical Lab. Techniques, College of Health & Medical Techniques, Imam Ja'afar Al-Sadiq University, Misan, Iraq*

[3] *Department of Chemical and Refining Petroleum Engineering, College of Oil and Gas Engineering, Basrah University for Oil and Gas, Basrah, Iraq*

[4] *Department of Chemistry, College of Education for Pure Sciences, University of Basrah, Basrah, Iraq*

ARTICLE INFO

Article History:
Received 22 April 2026
Accepted 13 August 2026
Published 01 October 2026

Keywords:
Carbon steel
Cinnamon (Cinnamomum verum)
Corrosion
Green synthesis
Silver nanoparticles

ABSTRACT

A green nano-inhibitor based on silver nanoparticles green-synthesized using *Cinnamomum verum* extract AgNPs.Cin was developed and evaluated for the corrosion protection of C45 carbon steel in 1.0 M HCl solution. The morphology of the synthesized nanoparticles was characterized by transmission electron microscopy (TEM) and field-emission scanning electron microscopy (FESEM). The corrosion inhibition performance was investigated using potentiodynamic polarization (PDP) and electrochemical impedance spectroscopy (EIS) at different inhibitor concentration and temperatures. The electrochemical result demonstrated that the inhibition efficiency increased with increasing inhibitor concentration but decreased with increasing temperature, reaching a maximum value of 94% at 500 ppm according to PDP measurements, while EIS measurements exhibited a maximum inhibition efficiency of 85% under the optimum experimental conditions. Adsorption studies revealed that the inhibitor followed the Langmuir adsorption isotherm, whereas thermodynamic and kinetic analyses suggested a spontaneous mixed adsorption mechanism involving both physisorption and chemisorption. The enhanced corrosion resistance was attributed to the adsorption of AgNPs.Cin constituents on the steel surface, the enhanced corrosion resistance was attributed to the adsorption of AgNPs.Cin constituents on the steel surface, and the electrochemical behavior is an adsorbed barrier that suppressed the corrosion process. Overall, the developed AgNP.Cin nano-inhibitor exhibited excellent corrosion protection performance highlighting its potential as an environmentally friendly and sustainable inhibitor for C45 carbon steel acidic environments

How to cite this article
Kadhim A., Shanta Alsadkhan A., Mohammed G. Cinnamon (Cinnamomum verum) Mediated Silver Nanoparticles as Green Corrosion Inhibitors for C45 Steel in Hydrochloric Acid. J Nanostruct, 2026; 16(4):5027-5053. DOI: 10.22052/JNS.2026.04.046

* *Corresponding Author Email: ayatjawdat@uomisan.edu.iq*

INTRODUCTION

Corrosion is an inevitable electrochemical process that result from oxidation-reduction reactions occurring at the interface between metallic materials and their surrounding environment. The rate and severity of corrosion are strongly influenced by environmental parameters such as temperature, pH, dissolved oxygen, humidity, electrolyte composition, and the presence of aggressive ions [1]. Under acidic conditions, particularly in hydrochloric acid (HCl) solution, the corrosion of metallic materials is significantly accelerated, leading to considerable material degradation and economic losses [2]. Carbon steel remains one of the most extensively utilized engineering materials in the petroleum and petrochemical industries because of its low cost, excellent mechanical strength, ease of fabrication, and widespread availability [3]. Despite these advantages, its relatively poor corrosion resistance in acidic environments restricts its long-term durability. During oil well acidizing, hydrochloric acid is routinely injected to dissolve carbonate scales and mineral deposits, thereby improving reservoir permeability and enhancing hydrocarbon production. However, this process simultaneously exposes steel pipelines, tubing and processing equipment to highly aggressive acidic media, substantially increasing corrosion rates and reducing service life [4,5]. Consequently, the development of efficient and economically viable corrosion protection strategies remains an important industrial and scientific objective.

Various approaches have been employed to mitigate metallic corrosion, including protective coatings, cathodic protection, alloy modification, and the addition of corrosion inhibitors [6]. Among these methods, corrosion inhibitors are considered one of the most practical and cost effective solution because only small concentration are required to substantially reduce metal dissolution. These compounds suppress anodic and cathodic electrochemical reaction by adsorbing onto the metal surface, thereby creating an adsorbed barrier that reduces the interaction between the substrate and the corrosive environment [7-10]. Depending on their chemical nature, corrosion inhibitors are generally classified into inorganic and organic compounds, the latter including both synthetic chemicals and naturally derived plant extracts [11,12].

Growing environmental concerns and increasingly stringent regulations have stimulated the search for sustainable alternatives to conventional synthetic inhibitors. Plant-derived corrosion inhibitors have attracted considerable attention because they are renewable, biodegradable, inexpensive, and generally exhibit low toxicity [13]. Their inhibition performance originates primarily from adsorption of naturally occurring phytochemical containing heteroatoms, aromatic ring, and π-electron systems onto metallic surface, resulting in the formation of adsorbed protective layers that reduce the corrosion reaction [14.15]. Nevertheless, although numerous plant extracts have demonstrated promising inhibition efficiencies, their practical performance is often limited by inadequate surface coverage, insufficient stability, and relatively weak adsorption under highly aggressive acidic conditions. These limitations have encouraged researchers to integrate green corrosion inhibition with nanotechnology to enhance adsorption efficiency, increase active surface area, and improve the durability of the protective layer.

Among the various plant resources investigated for green nanotechnology, *Cinnamomum verum* (cinnamon), a member of the Lauraceae family, has attracted considerable scientific interest because of its abundance of bioactive phytochemical and remarkable biological activities [16-18]. The bark of *Cinnamomum verum* is particularly rich in polyphenols, flavonoids, terpenoids, alcohols, esters, organic acids, and phenolic compounds such as eugenol and pyrogallol, which exhibit excellent antioxidant and reducing capabilities [19-21]. These naturally occurring phytochemical not only contribute to the medicinal value of cinnamon but also serve as efficient reducing and stabilizing agents during the green synthesis of metallic nanoparticles [22-24]. Consequently, plant-mediated synthesis has emerged as an environmentally sustainable alternative to conventional chemical methods by eliminating the need for toxic reducing agents while producing stable nanostructures.

Among metallic nanomaterials, silver nanoparticles AgNPs have received particular attention because of their high chemical stability, excellent surface reactivity, and exceptionally large surface area to volume ratio [25-27]. These characteristics enhance their adsorption capability and facilitate the development of an adsorbed surface layer on metallic surfaces, making them

promising candidates for corrosion inhibition applications [28]. Furthermore, combining AgNPs with phytochemical-rich plant extract is expected to generate a synergistic effect that improves nanoparticle stability, increases adsorption efficiency, and enhances corrosion protection under aggressive acidic conditions.

Although several plant extract have been investigated as green corrosion inhibitors, studies concerning green-synthesized silver nanoparticles derived from *Cinnamomum verum* for protecting carbon steel in hydrochloric acid remain limited. In particular, the relationship between nanoparticle physicochemical characteristics, electrochemical, behavior, adsorption performance, and inhibition mechanism has not yet been comprehensively established. Addressing these aspects is essential for understanding the protective action of green nanomaterials and expanding their practical applications in industrial corrosion control.

Accordingly, the present study aims to synthesize environmentally friendly silver nanoparticles using *Cinnamomum verum* extract AgNPs.Cin and to evaluate their corrosion inhibition performance for carbon steel in 1 M HCl solution. The synthesized nanoparticles were characterized using uv-Visible spectroscopy, FTIR, FESEM, and TEM analyses, while their corrosion inhibition performance was systematically investigated through potentiodynamic polarization and electrochemical impedance spectroscopy at different inhibitor concentration and temperatures. In addition, adsorption behavior, thermodynamic parameters, and kinetic characteristics were analyzed using the Langmuir adsorption isotherm, Arrhenius equation, and transition-state theory to elucidate the inhibition mechanism.

The novelty of this work lies in the development and evaluation of green synthesis AgNPs.Cin derived from Cinnamomum verum extract as a green corrosion inhibitor for C45 carbon steel in 1.0 M HCl. This study investigates the corrosion inhibition performance of this green-synthesized nanocomposite through physicochemical characterization, electrochemical evaluation, adsorption modeling, and thermodynamic and kinetic analysis. The obtained result provide a comprehensive evaluation of the corrosion inhibition performance of the green-synthesized AgNPs.Cin system and demonstrate its potential as a sustainable green corrosion inhibitor in acidic environments.

MATERIALS AND METHODS

The materials used in this research included dried cinnamon (Cinnamomum verum(silver nitrate ($AgNO_3$) (purchased from Merck, Germany), 1 M hydrochloric acid (HCl), and distilled water.

Plant extract preparation [29]

Dried cinnamon (*Cinnamomum verum*) was purchased from a local herbal market and authenticated based on its morphological characteristics. The dried cinnamon was finely

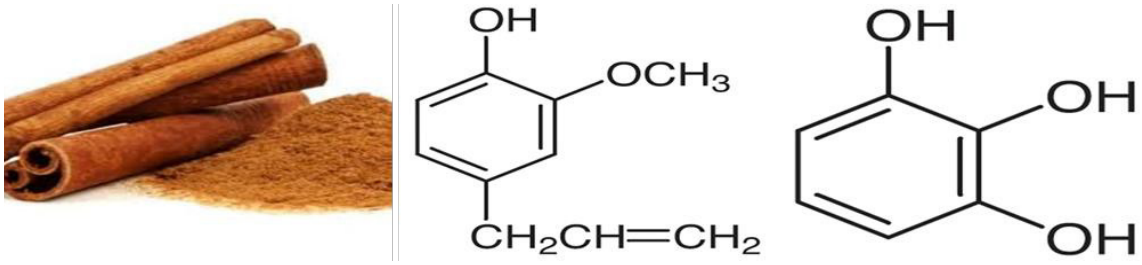

Fig. 1: Cinnamomum verum and Eugenol , Pyrogallol

Table 1. Chemical composition of carbon steel C45

Metal	C%	Si%	Mn%	S%	P%	Cu%	Ni%	Cr%	Fe%
Carbon Steel 45	0.36-0.42	0.15-0.30	1.00-1.40	0.05	0.05	0.50	0.20	0.20	96.88-97.49

ground, and 10 g of the powder was mixed with 100 ml of distilled water in a 250 ml conical flask. The mixture was heated at 80°C for 2 h and then filtered using filter paper. The obtain extract was stored 4°C and used immediately for the synthesis of silver nanoparticles.

Synthesis of silver nanoparticles (AgNPs.Cin)[30]

A 1 mM $AgNO_3$ solution was prepared by dissolving 0.1699 g of silver nitrite in 100 ml of distilled water. Subsequently, 50 ml of the prepared $AgNO_3$ solution was added dropwise to 5 ml of the cinnamon extract under magnetic stirring for 20 min. The volume ratio of $AgNO_3$ solution to cinnamon extract was 10:1 (v/v). The reaction temperature was maintained between 45°C and 50°C until the solution changed to a brown color, indicating the formation of silver nanoparticles AgNPs.Cin.

Scanning Electron Microscopy (FESEM)

FESEM pictures were obtained using a Field Emission Scanning Electron Microscopy, MIRA III, Tescan, Czech. at various magnification levels.

UV-Visible spectra

Ultraviolet Visible, 1900, Sgimadzu, Jaban was used to analyze the UV-visible spectra of silver nanoparticle citral 1mM. This indicates that it uses light in the visible and adjacent (near-UV and NIR) spectrums. Our perception of color is directly impacted by the absorption of molecules in the visible spectrum. Molecules go through electrical changes in this area of the visual spectrum.

Fourier Transform Infrared Spectroscopy (FT-IR)

FT-IR was used to identify the chemical bonds and functional groups of AgNPs. In a hydraulic press, pellets were made by combining KBr and AgNPs.Cin. It was examined in the 400–4000 cm^{-1} range using the Shimadzu 8400S Jaban FT-IR spectrometer.

Corrosion inhibition study

AgNPs.Cin synthesis using Cinnamomum verum (cinnamon) extract were utilized as the corrosion inhibitor. The reported concentration 100, 300, and 500 ppm refer to the synthesized AgNPs.Cin colloidal suspension used directly after the green synthesis process. The nanoparticles were neither isolated nor dried before preparing the test solutions. The blank solution consisted 50 ml of 1 M HCl. Carbon steel specimens were immersed in 1 M HCl containing (100, 300, 500) ppm of the AgNPs.Cin colloidal suspension for 7 hours temperature ranging from 298 to 318 K. Electrochemical measurements were carried out within a potential range of ± 200 mV.

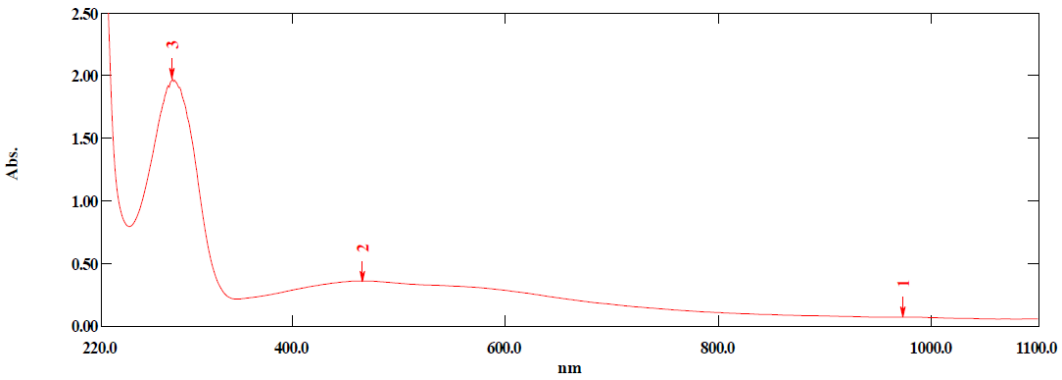

Fig. 2. UV-visible spectra of AgNPs.Cin

Table 2. UV-Visible Spectral Data of AgNPs.Cin

No	Wavelength(nm)	Abs.
1	973.0	0.069
2	465.0	0.358
3	287.0	1.973

Corrosion measurement

The potentiostat set up includes a Host computer, thermostat, magnetic stirrer, (EmStat 4s, Palm Sens, Holland) potentiostat, and galvanostat. The cell is (250) ml capacity made of Pyrex consist of internal and external bowls. The electrochemical corrosion cell is three electrodes. carbon steel as a working electrode used to determine the potential of it according to the reference electrode, an auxiliary electrode is a platinum with length (10)cm and reference electrode a saturated calomel (Hg/Hg_2Cl_2 sat. KCl). The working electrode was immersed in the test solution for 15 min to establish steady state open circuit potential (Eocp), then electrochemical measurements were performed in a potential range of (± 200) mV.

Polarization Curves

The corrosion current density (icorr) and corrosion potential (Ecorr) were obtained by the extrapolation of the cathodic and anodic Tafel in absence and presence the inhibitors molecules in HCl solution. Tafel plot reveals that Ecorr for C.S in the presence the inhibitors shifts to a higher (noble) position compared with blank solution, implying that the protection acts as an anodic protection. The inhibition efficiency (%IE) was calculated by the following equation [31,32].

$$\%IE = \frac{(icorr)o - (icorr)}{(icorr)o} * 100$$

Where $(I_{corr})_o$ is the corrosion current density in the absence of inhibitors, (I_{corr}) is the corrosion current density in the presence of inhibitors [33].

Chemical Composition of Carbon Steel C45

The chemical composition of the carbon steel C45 specimen employed in this work is summarized in Table 1. As can be seen, iron (Fe) represent the major component, while other elements such as carbon (C), silicon (Si), manganese (Mn), sulfur (S), phosphorus (P), copper (Cu), nickel (Ni), and chromium (Cr) are present in minor proportions, which may influence the corrosion behavior.

RESULTS AND DISCUSSION

The UV-visible spectra

Fig. 2 present the UV-visible spectrum of green-synthesized silver nanoparticles AgNPs. Cin prepared using *Cinnamomum* extract. The reaction mixture changed from pale yellow to dark brown after the addition of $AgNO_3$, indicating the reduction of Ag^+ ions and the formation of AgNPs.Cin. The spectrum exhibited a strong absorption band at 287 nm, attributed to the bioactive phytochemicals of the extract that acted as reducing and stabilizing agents. A broad absorption band at 465 nm corresponds to the localized surface Plasmon resonance (LSPR) of silver nanoparticles, confirming their successful formation [34].

Overall, the Uv-Visible results confirm are consistent with the successful green-synthesis of

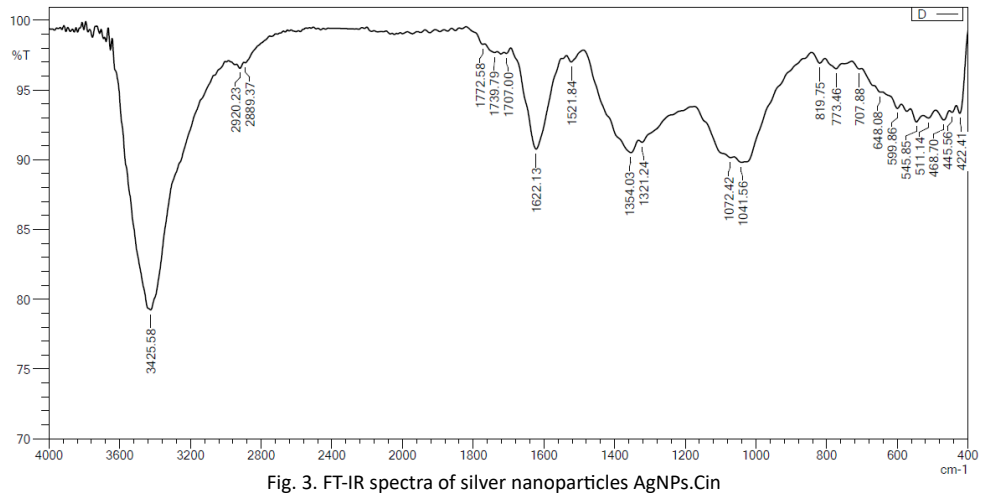

Fig. 3. FT-IR spectra of silver nanoparticles AgNPs.Cin

AgNPs.Cin using *Cinnamomum* extract, where the plant phytochemical promoted the reaction of A^{+} ions to metallic Ag^{0} while simultaneously stabilizing the formed nanoparticles. These findings are in good agreement with the results reported by Vijayan et al. [35], who also attributed the formation of silver nanoparticles to the reduction of Ag^{+} ions by plant-derived phytochemical during green synthesis.

FTIR spectrum

The FTIR spectrum of the AgNPs.Cin (Fig. 3) exhibits broad absorption band at 3425.58 cm^{-1}, Corresponding to O-H stretching vibrations of hydroxyl groups presnt in phenolic compounds. The bands at 2920.23 cm^{-1} and 2889.37 cm^{-1} were assigned to C-H stretching vibrations of aliphatic groups. The absorption bands observed at 1773-1707 cm^{-1} were attributed to C=O stretching vibrations of carbonyl-containing compounds, while the band at 1622 cm^{-1} was associated with C=C stretching vibrations of aromatic rings and conjugated carbonyl groups. The bands at 1354 and 1321 cm^{-1} were assigned to C-N and O-H bending vibrations, whereas the band at 1072 and 1042 cm^{-1}corresponded to C-O stretching vibrations of alcohols, ethers, and phenolic compounds. These spectral features are consistend with the presence of phytochemical constituents from the cinnamon extract and suggest the possible involvement of hydroxyl, carbonyl, carboxylate, and related oxygen-containing functional groups in the reduction of Ag^{+} ions [36,37]. However, because FTIR analysis was performed only on the finl AgNPs.Cin product without direct comparison with the original cinnamon extract, washed nanoparticles, or reference compounds, these assignments should be regarded as supportive rather than conclusive evidence of their role in the green-synthesis process.

FE-SEM analysis

Surface Morphology and Structural Features Analysis

The surface topography, microstructure, and morphological characteristics of the green-synthesized AgNPs.Cin were comprehensively scrutinized using Field Emission Scanning Electron Microscopy (FE-SEM). The obtained FE-SEM micrographs at different magnifications provide crucial insights into the morphological characteristics and growth mechanism of the green-synthesized AgNPs.Cin, as illustrated in Fig. 4.

At a moderate magnification of 15.00 KX Fig. 4a. the FE-SEM micrograph unveils a highly continuous, interconnected, and porous network. The topography exhibits a homogenous and uniform distribution of the synthesized nanomaterials over a wide scanned area, implying the efficacy of the green synthesis approach in producing a well-dispersed matrix [38]. The observed micro-porosity and rough surface architecture are highly advantageous for various technological, as they significantly increase the effective surface-area-to-volume ratio [39].

To gain a deeper understanding of the distinct nanostructures, a high-magnification FE-SEM characterizations was performed at 80.00 KX Fig. 4b. The high-resolution image indicates that the

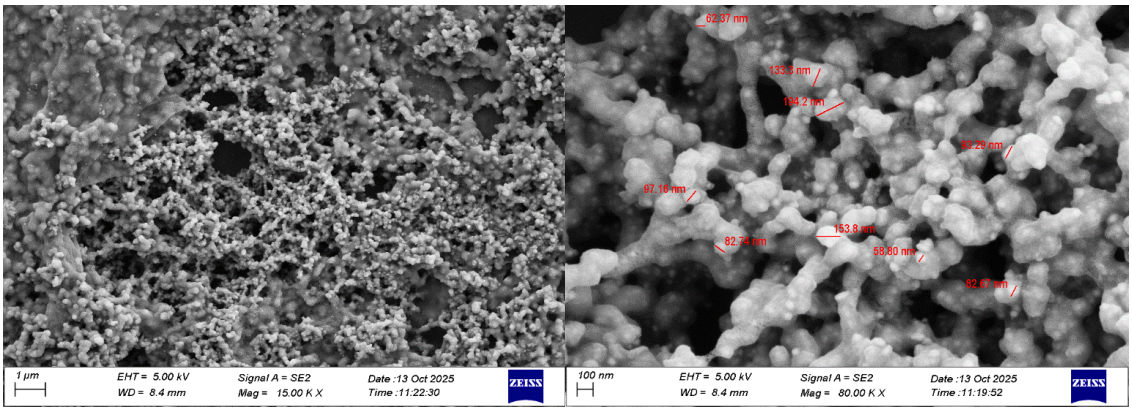

Fig. 4. FESEM of AgNPs.Cin

fabricated AgNPs.Cin possess a predominantly spherical to quasi-spherical morphology. This spherical geometry is thermodynamically favored during the nucleation and growth stages of silver ions (Ag^{+} to Ag^{0}), as it minimizes the surface free energy [40].

The FE-SEM images reveal nanoscale features with apparent particle diameters ranging from approximately 58.80 nm to 133.3 nm. However, some large structures reaching approximately 194.2 nm are observed, which are mainly attributed to nanoparticle aggregation. This agglomeration is a characteristic phenomenon in green synthesis protocols [41]. It can be scientifically attributed to the presence of secondary metabolites and bioactive macromolecules within the cinnamon extract, such as cinnamaldehyde, eugenol, and polyphenols. These biomolecules act not only as potent reducing agents but also as capping and stabilizing agent (Capping ligands). The bio molecular coating forms a surrounding organic matrix that bridges the adjacent nanoparticles, resulting in the observed branch-like cluster morphology [42].

The structural features revealed by this FE-SEM study indicate *Cinnamomum verum* extract provides an effective, eco-friendly biogenic route for the controlled synthesis of silver nanoparticles

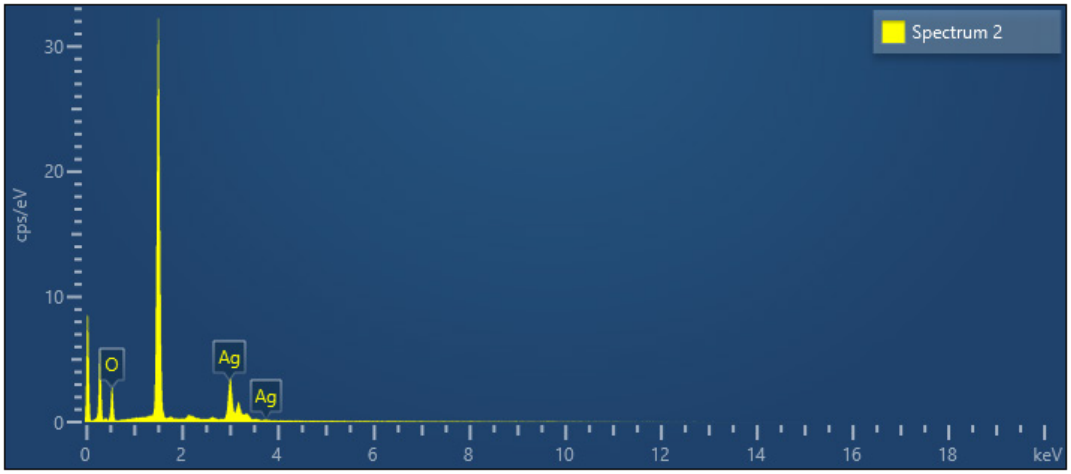

Fig. 5. EDX analysis of synthesized AgNPs.Cin Description of corrosion system.

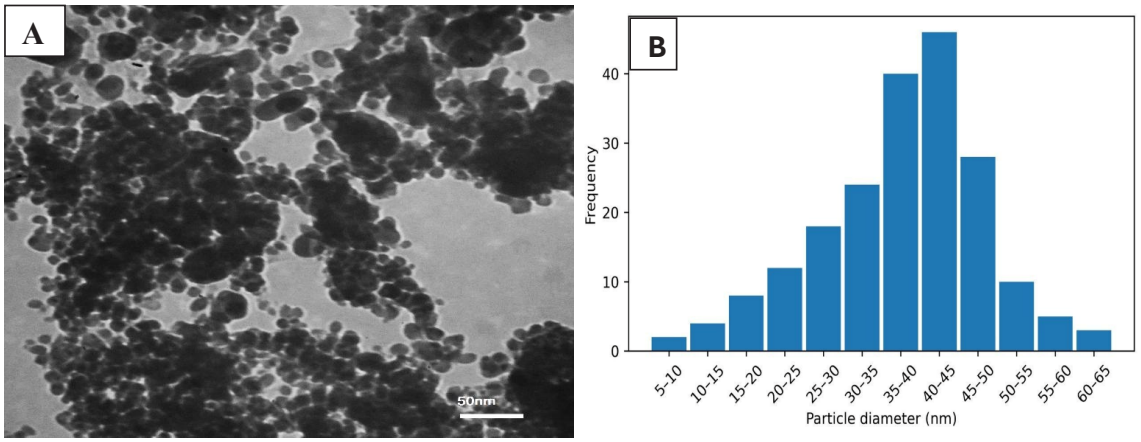

Fig. 6. (A) TEM micrograph of green-synthesized silver nanoparticles prepared using cinnamon extract, showing nanoparticle morphology and agglomeration, (B) Particle-size distribution histogram of the synthesized AgNPs.Cin obtained from TEM image analysis

[43].

Elemental Composition Analysis (EDX)

The EDX spectrum of the spectrum of the synthesized AgNPs.Cin is shown in Fig. 5. A prominent peak is observed at approximately 3 KeV, corresponding to the characteristic AgLα emission of metallic silver, confirming the presence of silver in the synthesized sample [44]. Additional Ag peaks with lower intensities are also observed, supporting the identification of silver [45]. A low-intensity oxygen (O) peak is detected at lower energy. The EDX spectrum confirms the elemental composition of the synthesized AgNPs. Cin [46,47].

Transmission Electron Microscopy (TEM) Analysis

The TEM micrograph is consistent with the successful green synthesis of silver nanoparticles AgNPs.Cin using cinnamon extract. The nanoparticles exhibit predominantly spherical to quasi-spherical morphologies, and are distributed within the nanoscale rang Fig. 6A. The strong electron-dense contrast is consistent with presence of silver nanoparticles. Noticeable nanoparticle agglomeration is also observed, which is commonly reported for plant-mediated AgNPs and is mainly attributed to the high surface energy of silver nanoparticles, antiparticle attractive forces, drying effects during TEM sample preparation, and interactions between, phytochemical capping molecules [48]. The corresponding particle-size distribution histogram Fig. 6B shows that most nanoparticles are within the 30-50 nm range, with the highest frequency observed between 40 and 45 nm, while fewer particles are found at smaller and larger size ranges. Overall the observed morphology, particle-size distribution, and aggregation behavior are consistent with previous reports on green-synthesized AgNPs. Cin and indicate the successful formation of nano sized silver particles with characteristics that may be favorable for corrosion inhibition [49].

Description of corrosion system

Potentiodynamic Polarization (PDP) measurements

Potentiodynamic Polarization (PDP) measurements were carried out using a conventional three-electrode electrochemical cell connected to a potentiostat/galvanostat system. The electrochemical cell was made of Pyrex glass with a total capacity of 250 ml and consisted of inner and outer compartments. A carbon steel specimen with an exposed surface area of 1 cm^2 was used as the working electrode. Reference electrode a saturated calomel electrode (SCE, Hg/Hg_2Cl_2/saturated KCl), positioned approximately 2mm from the working electrode minimize the ohmic potential drop, while platinum rod (10 cm) served as the counter electrode. The experimental temperature was maintained using a thermostatic cooling-heating circulating water bath throughout the measurement.

Prior to each experiment, the exposed surface of the carbon steel specimen was polished using silicon carbide (SiC) abrasive paper, degreased with acetone, rinsed twice with distilled water, and allowed to try at room temperature. The working electrode was then immersed in the test solution for 15 min to allow the open circuit potential (OCP) to reach a steady before polarization measurements. PDP measurements were subsequently performed over a potential rang of ±200 mV relative to the OCP at a scan rate of 1.0

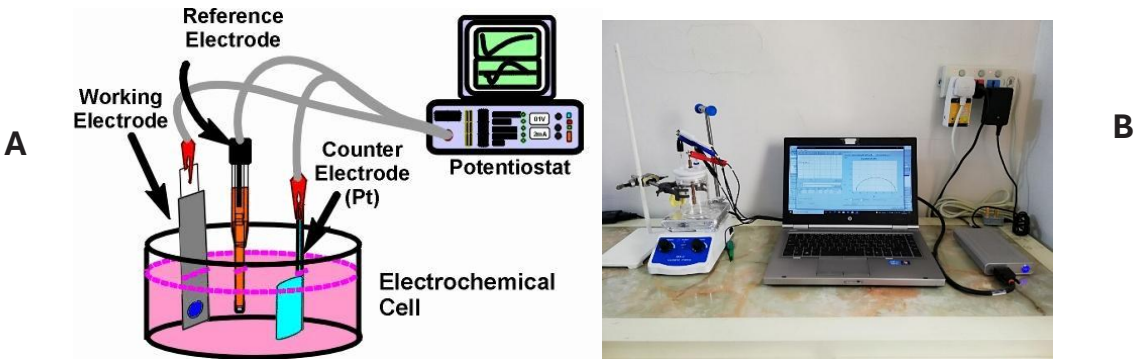

Fig. 7. (A) Schematic diagram of the electrochemical cell, (B) Experimental EIS measurement setup

mV/s in 1.0 M HCl solution containing different concentration of AgNPs. All electrochemical measurements were conducted in triplicate under identical experimental conditions, and the reported values represent the average of three independent measurements. Fig. 7A.

Electrochemical Impedance Spectroscopy (EIS) Measurements

Electrochemical impedance spectroscopy (EIS) measurements were carried out using a computer-controlled potentiostat/galvanostat system coupled with a conventional three-electrode Pyrex electrochemical cell (100 ml capacity) as shown in Fig. 7B. The C45 carbon steel specimen served as the working electrode with an exposed surface area of 1 cm^2, while a saturated calomel electrode (SCE, Hg/Hg_2Cl_2/saturated KCl) and a high-purity platinum electrode (1 cm^2) were used as the reference and counter electrodes, respectively.

Prior to each experiment, the working electrode was sequentially with 200, 600, and 1200 grit silicon abrasive papers, rinsed thoroughly with deionized water, washed with ethanol, and dried before immersed in the test solution. The working electrode was immersed in the electrolyte for 15 min to allow the open-circuit potential (OCP) to reach a steady state before each measurement. EIS measurement were carried out by applying a sinusoidal AC perturbation with an amplitude of 10 mV over a frequency rang of 0.1 Hz to 100 Hz. The impedance spectra were analyzed using PSTrace 5.12 soft were and fitted with the equivalent electrical circuit Rs-(Q‖Rct) to obtain the solution resistance (Rs), charge transfer resistance (Rct), and constant phase element (CPE) (Fig. 7B).

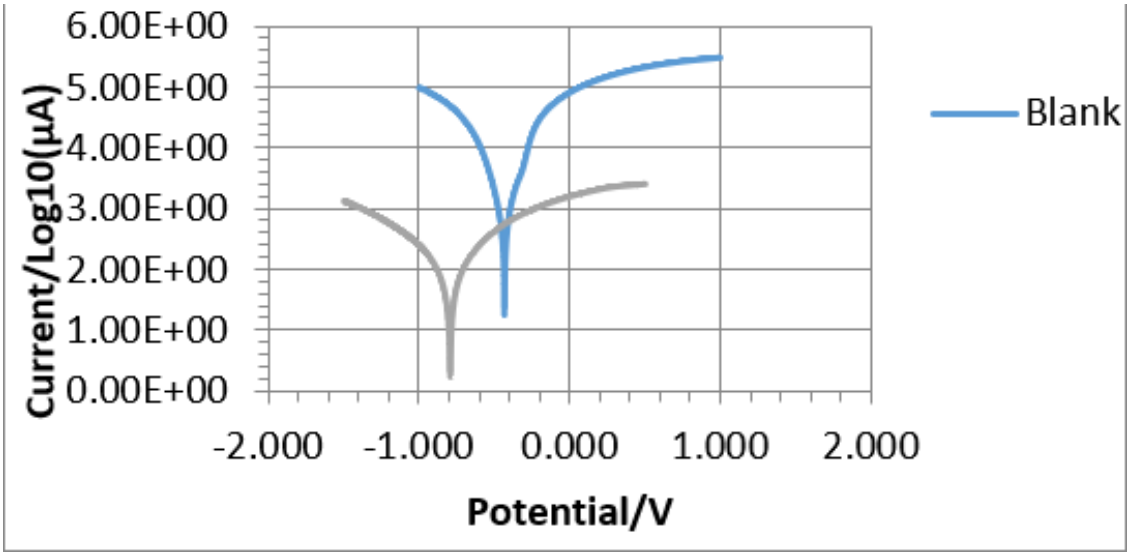

Fig. 8. Polarization curves for corrosion of blank HCl + AgNPs.Cin.

Table 3. Corrosion parameters for blank and compound in HCl solutions and different compound

Comp.	blank	AgNPs.Cin
-Ecorr (mV)	-0.427	-0.792
Icorr (µA/cm^2)	493.9	46.62
Resis. (Ω)	70.31	2217
-Bc (mV/Dec)	0.156	0.455
Ba (mV/Dec)	0.164	0.499
Corr. rate, (mm/y)	5.744	0.458
IE%	-	91

Potentiodynamic Polarization Analysis (PDP) Tafel Potentiodynamic polarization (PDP) measurements were performed to evaluate the corrosion inhibition performance of the green-synthesized AgNPs.Cin toward C45 carbon steel 1M HCl solution. The electrochemical parameters obtained from the polarization curves, including the corrosion potential (E_{corr}), corrosion current

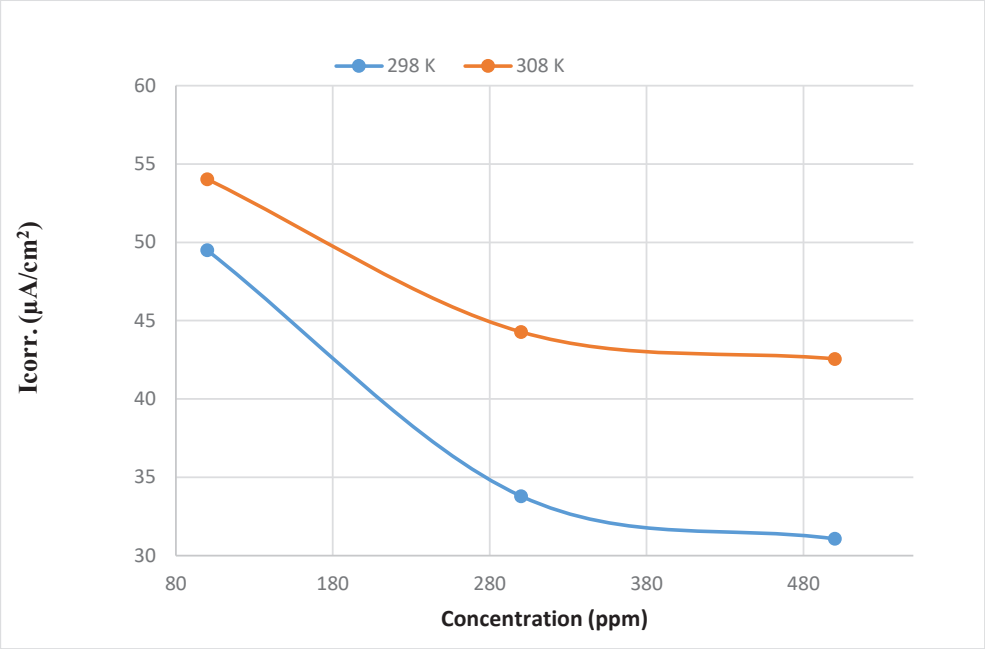

Fig. 9. The impact of varying inhibitor AgNPs.Cin doses at temperatures between 298K and 308K on the corrosion current density in acidic solutions

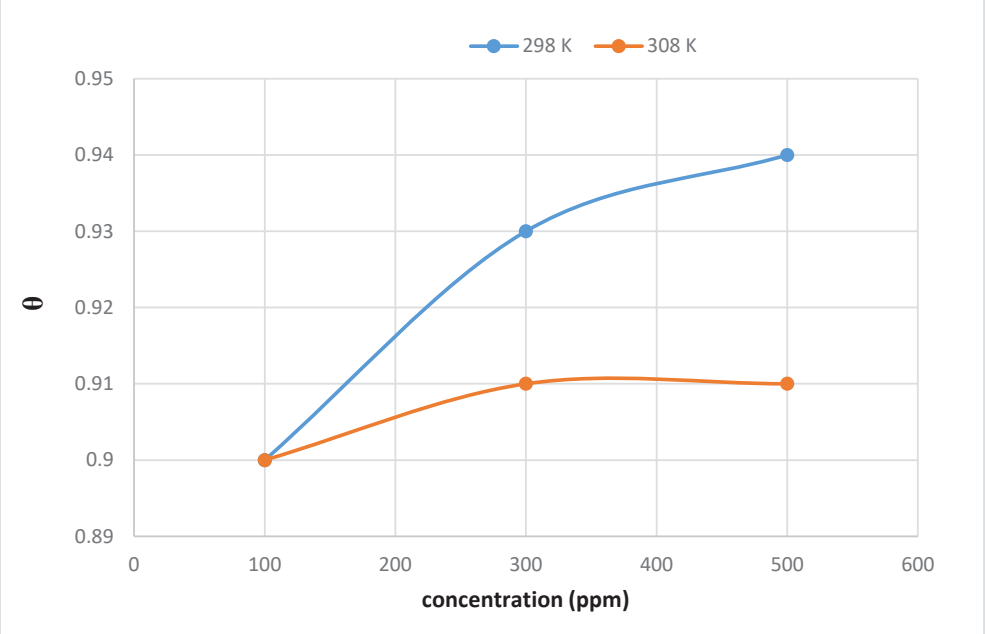

Fig. 10. Impact of varying concentration at 298–308 K degrees on the area of the section covered by the inhibitor AgNPs.Cin

density (I_{corr}), anodic and cathodic Tafel slopes (β_a and β_c), polarization resistance (Rp), corrosion rate (CR), and inhibition efficiency (IE%), are summarized in Table 3, while the corresponding polarization curves are presented in Fig. 8. The addition of AgNPs.Cin markedly altered the polarization behavior of C45 carbon steel compared with the uninhibited solution. The corrosion current density decreased substantially from 493.9 µA/cm² to 46.62 µA/cm² demonstrating a significant reduction in the electrochemical corrosion reaction. Simultaneously, the polarization

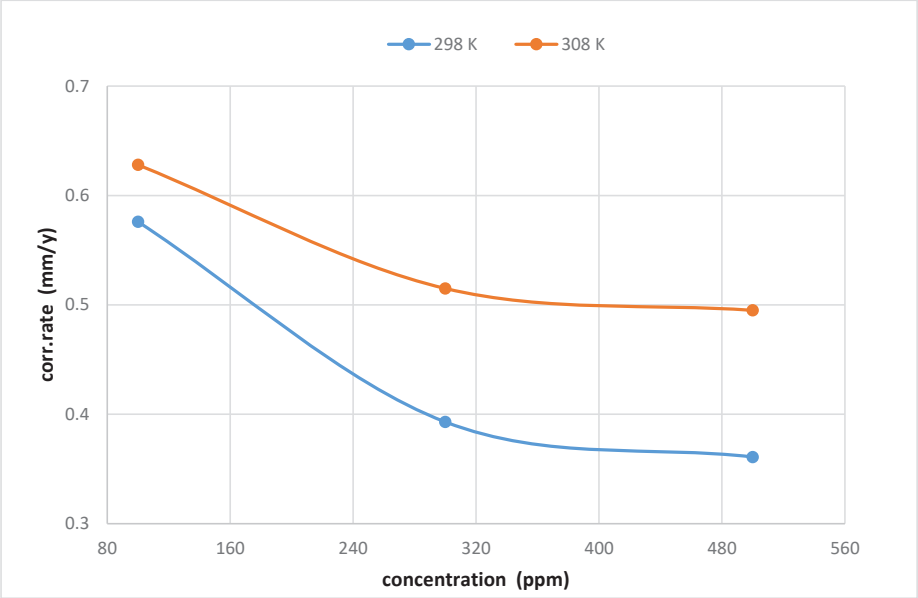

Fig. 11. Impact of concentration variation on the rate of corrosion at 298–308 K

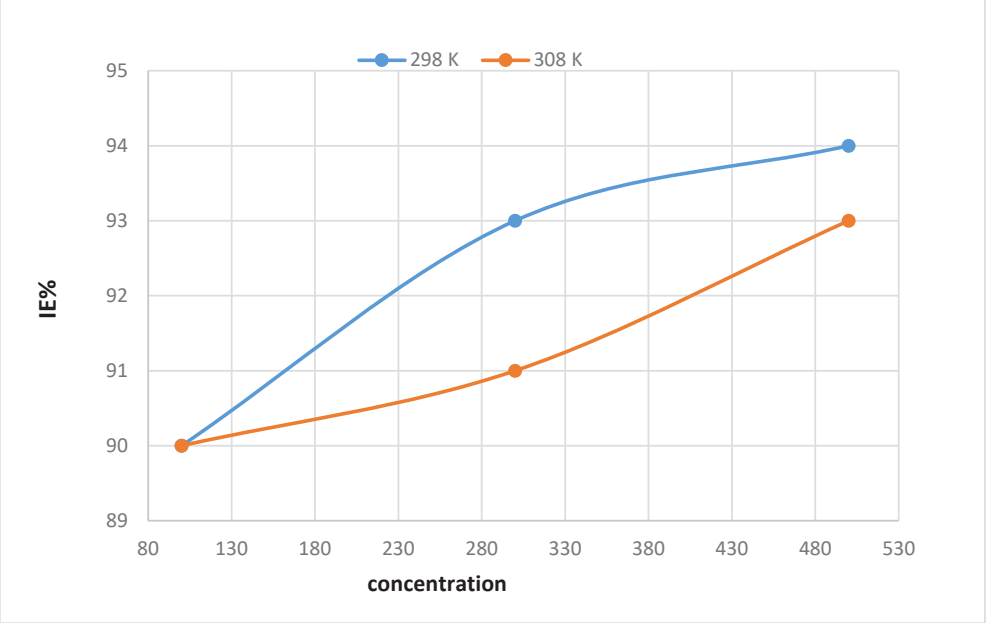

Fig. 12. Impact of concentration variation on the inhibitor's AgNPs.Cin inhibitory effectiveness at 298–308 K

resistance increased remarkably from 70.31 Ω to 2217 Ω, suggesting the formation of an adsorbed protective layer on the steel surface, which is consistent with hindered charge transfer across the metal/electrolyte interface. Consequently, the corrosion rate decreased from 5.744 mm/y to 0.458 mm/y, resulting in an inhibition efficiency of approximately 91%, which demonstrates the excellent protective performance of the synthesized AgNPs.Cin.

The displacement of the corrosion potential E_{corr} provides useful information regarding the influence of the inhibitor on the anodic and cathodic reaction. Generally, inhibitors are

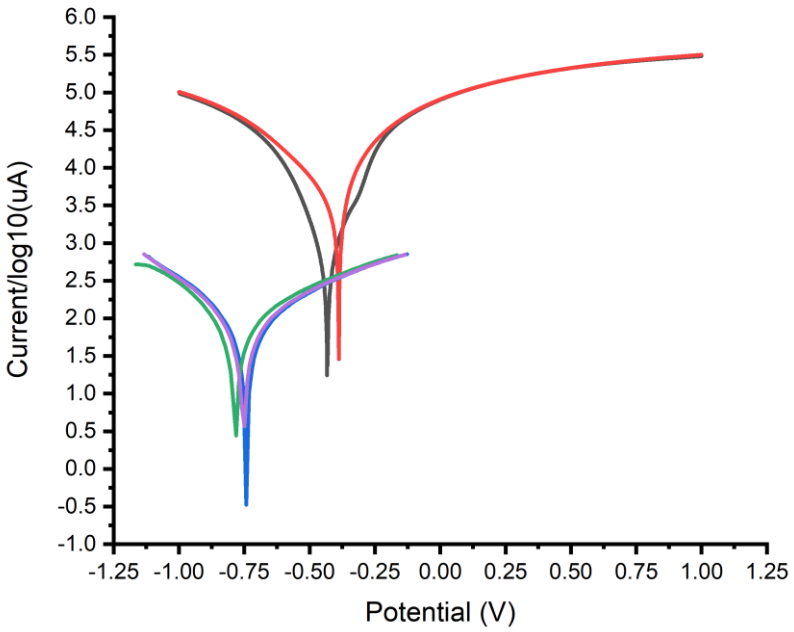

Fig. 13. Show the polarization curves for carbon steel corrosion at 298 K with and without inhibitor AgNPs.Cin

Table 4. Potentiodynamic polarization parameters of C45 carbon steel in 1 M HCl containing different concentrations of AgNP.Cin at 298 and 308 K

Comp.	Blank		100 ppm		300 ppm		500 ppm	
Temp. (K)	298	308	298	308	298	308	298	308
-Ecorr. (mV)	-0.427	-0.385	-0.729	-0.741	-0.764	-0.744	-0.746	-0.733
Icorr. (μA/cm²)	493.9	563.2	49.49	54.03	33.80	44.28	31.07	42.56
Resis (Ω)	70.31	28.96	1312	1308	1291	1329	1329	1355
-Bc (mV/Dec)	0.156	0.055	0.305	0.356	0.205	0.286	0.190	0.273
-Ba (mV/Dec)	0.164	0.120	0.298	0.300	0.197	0.258	0.191	0.259
Corr.rate (mm/y)	5.744	6.550	0.576	0.628	0.393	0.515	0.361	0.495
θ	-	-	0.90	0.90	0.93	0.91	0.94	0.91
IE%	-	-	90	90	93	91	94	93

classified as anodic, cathodic, or mixed-type according to the magnitude of the E_{corr} shift in comparison with the uninhibited solution [50-53]. As illustrated in Fig. 7A, the presence of AgNPs. Cin reduced both anodic metal dissolution and the cathodic hydrogen evolution reaction, indicating that the inhibitor effectively suppressed the overall corrosion process through simultaneous modification of both electrochemical reactions [54,55]. These findings, together with the pronounced decrease in corrosion current density and the significant increase in polarization resistance, suggest that the corrosion inhibition performance is associated with adsorption of AgNPs.Cin on the carbon steel surface, resulting in electrochemical behavior consistent with the formation of an adsorbed barrier in acidic media. E corrosion, I corrosion, µA, Polarization Resistance, Ω, Anodic β Tafel constant, V/decade, Cathodic β Tafel constant, V/decade, Corrosion rate, mm/year, IE% inhibition efficiency.

To calculate the degree of surface covering(Θ) by the inhibitor, use the following equation:

$$\theta = \frac{\text{Icorr. uninh} - \text{Icorr. inh}}{\text{Icorr. uninh}}$$

Icorr.uninh = Corrosion current density without inhibitor, Icorr.inh = Corrosion current density in the presence of inhibitor.

By applying the above equation to the current values, we obtain the area of the part covered by the inhibitor, which is equal to θ = 0.91.

Effect of inhibitor concentration and temperature on the corrosion inhibition performance

The influence of AgNPs.Cin concentration and temperature on the corrosion behavior of carbon steel in 1M HCl was evaluated using potentiodynamic polarization measurements, and the obtained electrochemical parameters are summarized in Table 4. As the inhibitor concentration increased from 100 to 500 ppm, the corrosion current density I_{corr} decreased markedly at both investigated temperatures 298 and 308 K, indicating progressive suppression of the electrochemical corrosion process. This behavior was accompanied by a continuous increase in surface coverage (θ) and inhibition efficiency (IE%), confirming the concentration-dependent inhibition performance of AgNPs.Cin Figs. 9-12.

At 298 K, increasing the inhibitor concentration from 100-500 ppm reduced I_{corr} from 49.49 µA/cm^2 to 31.07 µA/cm^2, while the inhibition efficiency increased from 90% to 94%, with the surface coverage rising from 0.90 to 0.94. A similar trend was observed at 308 K, although the inhibition efficiency was slightly lower, reaching 93% at the highest concentration. Simultaneously, the corrosion rate decreased markedly in the presence of the inhibitor, demonstrating the

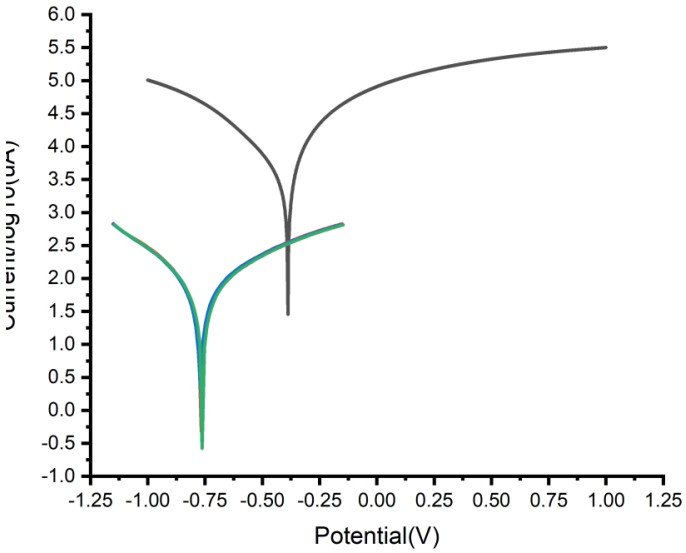

Fig. 14. Show the polarization curves for carbon steel corrosion at 308 K with and without inhibitor AgNPs.Cin

effective corrosion inhibition performance of the synthesized nanomaterial compared with the uninhibited solution.

The enhanced inhibition performance at higher inhibitor concentrations may be attributed to the increased adsorption of AgNPs.Cin species onto the carbon steel surface, leading to greater inferred surface coverage and more effective blocking of the active corrosion sites [56-58]. Consequently, the corrosion current density (I_{corr}) decreased progressively with increasing inhibitor concentration, while the inhibition efficiency (%IE) and surface coverage (θ) increased accordingly. These results indicate that increasing the inhibitor concentration improves the protection of carbon steel against the aggressive hydrochloric acid medium[59-60].

Increasing the solution temperature from 298 to 308 K resulted in a slight increase in the corrosion current density and corrosion rate, accompanied by a marginal decrease in inhibition efficiency and surface coverage. Nevertheless, AgNPs.Cin maintained high inhibition efficiency even at 308 K, demonstrating its effective corrosion protection over the investigated temperature range [61-63].

The polarization curves presented in Figs. 13 and 14 further support these findings. The addition of AgNPs.Cin significantly reduced the corrosion current density I_{corr}, confirming its effective corrosion inhibition performance. Both the anodic and cathodic polarization branches exhibited lower current densities in the presence of the inhibitor, indicating that the inhibitor influenced both electrochemical reactions and significantly reduced the overall corrosion rate [64].

Study of the Adsorption Isotherm of AgNPs.Cin on Carbon Steel Surface

The corrosion inhibition performance of AgNPs.Cin is primarily attributed to the adsorption of inhibitor molecules onto the carbon steel surface, leading to the proposed formation of an adsorbed protective layer that reduces the interaction between the metal surface and the aggressive acidic environment. During the adsorption process, inhibitor molecules progressively replace the water molecules initially adsorbed on the metal surface through a substitution mechanism, which

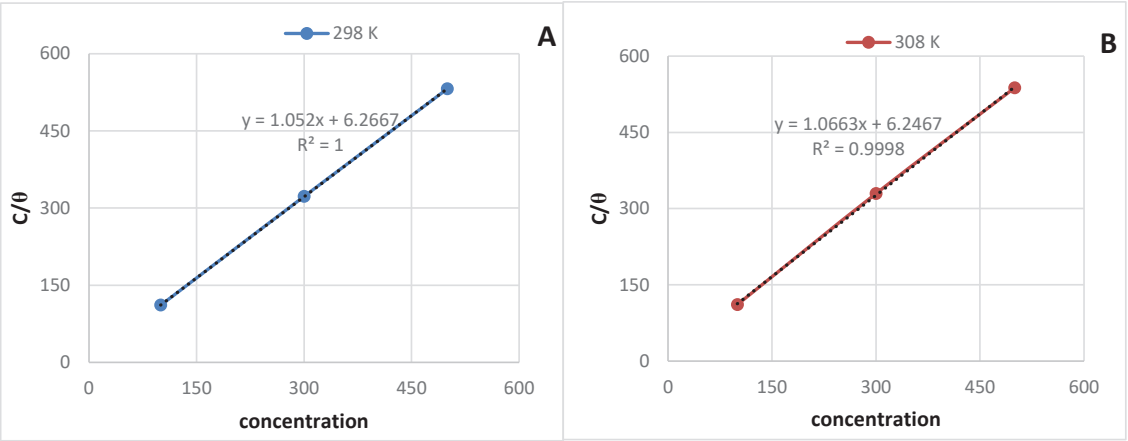

Fig. 15. Isotherm relationship for Langmuir in different concentrations of inhibitors AgNPs.Cin, (A) at 298K, (B) at 308K

Table 5. Shows the correlation coefficient, adsorption constant and adsorption functions of inhibitors on carbon steel alloy.

T	R	K_{ads}	ΔG°_{ads} (KJ.mol^{-1})
298	1	0.1596	-29.68
308	1	0.1601	-30.69

can be represented by the following equilibrium [65].

$$Inhibitor_{sol} + xH_2O_{ads} \rightleftharpoons Inhibitor_{ads} + xH_2O_{sol}$$

Adsorption isotherm analysis provides valuable information regarding the interaction between inhibitor molecules and the metal surface, allowing the adsorption mechanism to be evaluated as physical, chemical, or mixed. Among the various adsorption models examined, the Langmuir adsorption isotherm provided the best fit for the experimental data at both 298 and 308 K, according to the following equation [66,67].

$$\frac{C_{inh}}{\theta} = \frac{1}{K_{ads}} + C_{inh}$$

The Langmuir plots shown in Fig. 15a-b exhibit excellent linear relationships with correlation coefficients of 1.0000 and 0.9998 at 298 and 308 K respectively. While the calculated slopes (1.052 at 298 K 1.0663 at 308 K) are very close to unity. These results demonstrate that the adsorption behavior of AgNPs.Cin is well described by the Langmuir adsorption model, suggesting adsorption consistent with a predominantly monolayer coverage on energetically equivalent active sites of the carbon steel surface [68].

The adsorption equilibrium constants K_{ads} calculated from the intercept values of the Langmuir plots were 0.1596 and 0.1601 at 298K and 308 K, respectively Table 5. The corresponding standard free energies of adsorption ΔG_{ads}° were -29.68 and -30.69 KJ/mol, respectively. The negative values ΔG_{ads}° indicate that the adsorption proceeds is spontaneous. In addition, the magnitude of ΔG_{ads}° is consistent with a mixed adsorption mechanism, involving both physical and chemical interactions between the inhibitor species and the carbon steel surface.

Based on the parameters of the equilibrium constant of the K_{ads} process, we can compute the free energy ΔG_{ads}° of compression using equation No. 5 [69] Table 5. Here, C_w represents the concentration of water, which was taken as 10^6 mg/L.

$$\Delta G_{ads}^{\circ} = -RTln(C_w . K_{ads})$$

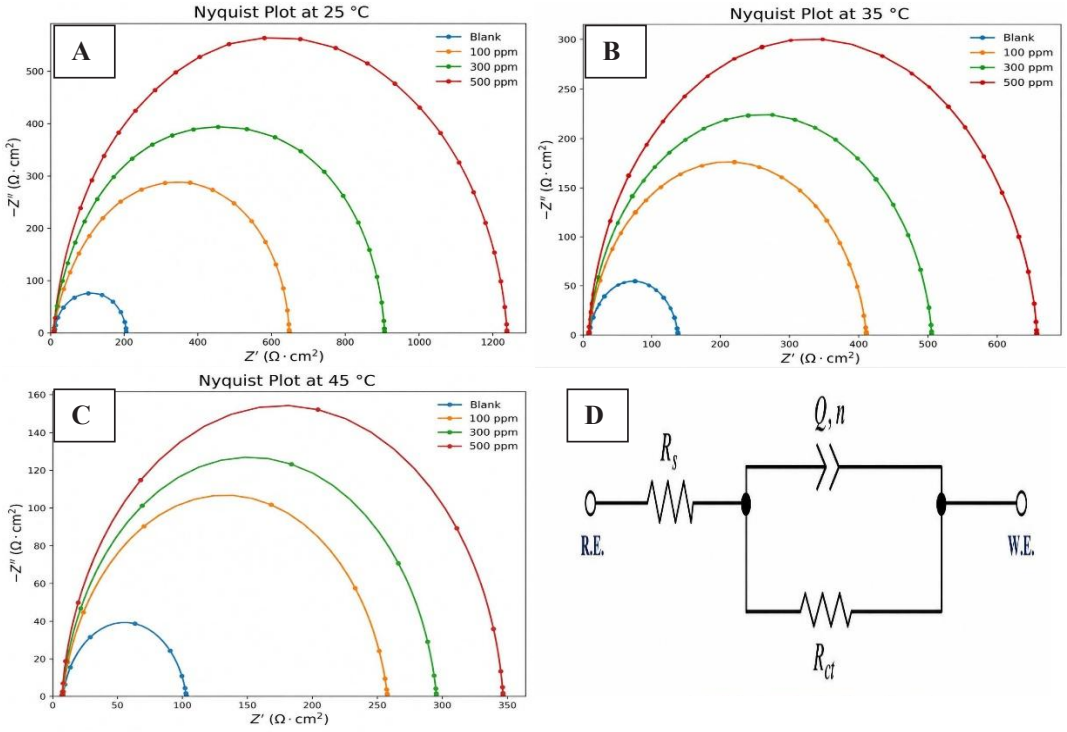

Fig. 16. Nyquist plots of carbon steel in 1 M HCl containing different concentration of AgNPs.Cin (A) 25°C (298), (B) 35°C (308), (C) 45°C (318), together with the equivalent electrical circuit (D) used for fitting the EIS data.

Electrochemical Impedance Spectroscopy (EIS)
Nyquist plot and electrochemical

The Nyquist plots obtained at 298, 308 and 318 K Fig. 16A-C, exhibit a single depressed capacitive semicircle for both the uninhibited solution and all AgNPs.Cin concentrations, indicating that the corrosion process is predominantly governed by a single charge-transfer mechanism. Accordingly, the experimental data were satisfactorily fitted using the equivalent circuit shown in Fig. 16D. The depressed nature of the semicircles reflects surface heterogeneity and non-ideal capacitive behavior arising from surface roughness and frequency dispersion, therefore, a constant phase element (CPE) was employed instead of an ideal capacitor, as commonly reported for corroding steel surfaces [70].

The addition of AgNPs.Cin markedly increased the diameter of the capacitive semicircle, and this enlargement became more pronounced as the inhibitor concentration increased from 100 to 500 ppm, demonstrating a progressive increase in charge-transfer resistance, consistent with adsorption of the nanoparticle-based inhibitor on the steel surface [71,72]. In contrast, increasing the temperature from 298 to 318 K reduced the semicircle diameter for all system, reflecting the acceleration of corrosion kinetic at elevated temperature [73]. Nevertheless, the inhibited solution retained significantly larger semicircles than the blank, indicating that AgNPs.Cin remained effective even at 318 K.

Charge-transfer resistance and inhibition efficiency

The electrochemical parameters summarized in Table 6 support the Nyquist observation. At 298 K, the charge-transfer resistance (Rct) increased from 180 $\Omega.cm^2$ for the blank solution to 642.86, 857.14 and 1200 $\Omega.cm^2$ after the addition of 100, 300 and 500 ppm AgNPs.Cin, corresponding to inhibition efficiencies of 72, 79 and 85%, respectively. The continuous increase in R_{ct} is consistent with increased surface coverage by the adsorbed inhibitor, leading to more effective blocking of active corrosion sites and suppression of both iron dissolution and hydrogen evolution reactions [74]. Increasing the temperature led to a gradual decrease in both R_{ct} and inhibition efficiency. At 500 ppm, the inhibition efficiency decreased from 85% (298 K) to 80% (308K) and 72% (318K), while the blank R_{ct} decreased from 180 to 95 $\Omega.cm^2$. This behavior indicates that higher temperature facilitate charge-transfer reactions and suggesting partial desorption adsorbed inhibitor at elevated temperature [75].

Table 6. Electrochemical impedance spectroscopy EIS parameters for carbon steel in 1M HCl solution in the absence and presence of different concentration of AgNPs.Cin at different temperatures

system	T (K)	Rs ($\Omega\cdot cm^2$)	Rct ($\Omega\cdot cm^2$)	Q ($F\cdot s^{n-1}\cdot cm^{-2}$)	n	Cdl ($\mu F\cdot cm^{-2}$)	IE (%)
BLANK	298	9.00	180.00	9.50×10^{-5}	0.90	60.45	—
	308	8.50	130.00	1.15×10^{-4}	0.89	68.41	—
	318	8.00	95.00	1.40×10^{-4}	0.87	77.68	—
100 ppm	298	8.80	642.86	7.20×10^{-5}	0.92	55.12	72.00
	308	8.30	406.25	8.80×10^{-5}	0.91	63.30	68.00
	318	7.80	250.00	1.12×10^{-4}	0.90	75.28	62.00
300 ppm	298	8.60	857.14	6.10×10^{-5}	0.94	50.53	79.00
	308	8.10	500.00	7.60×10^{-5}	0.93	59.42	74.00
	318	7.60	287.88	9.80×10^{-5}	0.92	71.86	67.00
500 ppm	298	8.40	1200.00	5.00×10^{-5}	0.96	44.47	85.00
	308	7.90	650.00	6.40×10^{-5}	0.95	54.14	80.00
	318	7.40	339.29	8.40×10^{-5}	0.94	66.93	72.00

Constant phase element and double-layer capacitance

Additional evidence for inhibitor adsorption is provided by the CPE exponent (n) and the calculated double-layer capacitance (Cdl). The n values increased from 0.87-0.90 to 0.92-0.96 after inhibition addition, indicating a more homogeneous metal/solution interface, consistent with adsorption of the inhibitor on the steel surface [76,77]. Meanwhile, Cdl decreased progressively as the inhibitor concentration increased. At 298 K, Cdl decreased from 60.45 µF/cm^2 for the blank solution to 55.12, 50.53 and 44.47 µF/cm^2 at 100, 300, and 500 ppm, respectively. Although Cdl increased with increasing temperature for all tested systems, it remained consistently lower than that of the uninhibited solution [78]. This reduction in Cdl attributed to the displacement of adsorbed water molecules and chloride ions by the phytochemical constituents of the cinnamon-derived silver nanoparticles, together with an increase in the thickness of the electrical double layer [79]. These finding are consistent with increased surface coverage by the adsorbed inhibitor, as reflected the increase in R_{ct} and the corresponding improvement in inhibition efficiency.

Results and Discussion Arrhenius Analysis of the Corrosion Process

As shown in Fig. 17, because EIS measurement were performed at three temperature, $1/R_{ct}$ was used as a surrogate apparent electrochemical kinetic parameter because it is inversely related to the charge-transfer resistance rather than being treated as an exact corrosion rate. Consequently,

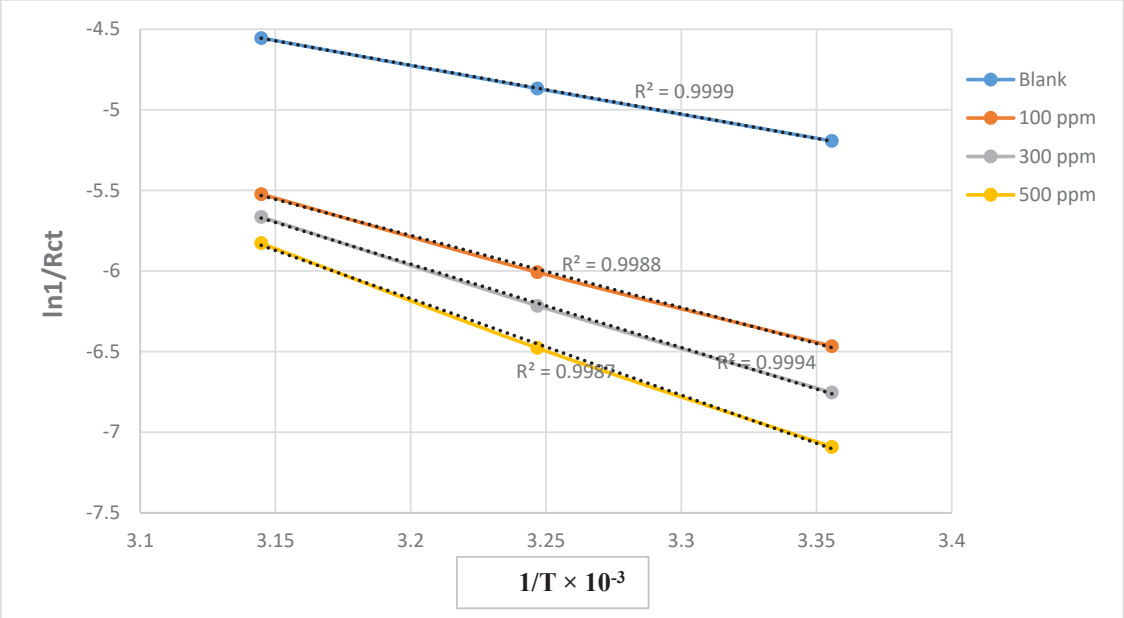

Fig. 17. Arrhenius plot [ln($1/R_{ct}$) vs 1/T] for carbon steel corrosion in the blank and inhibited solution at different concentrations

Table 7. Apparent activation energy (Ea) and pre-exponential factor (A) for carbon steel corrosion in the blank and inhibited solution

System	Ea (KJ/mol)	A	R^2
Blank	25.2	1.4×10^2	0.9999
100 ppm	37.2	5.1×10^3	0.9988
300 ppm	43.0	3.9×10^4	0.9994
500 ppm	49.7	1.2×10^6	0.9987

the calculated activation energies represent apparent electrochemical activation energies. Accordingly, the following apparent Arrhenius relationship was used [80,81]:

$$\ln(1/R_{ct}) = \ln(A) - Ea/RT$$

where R_{ct} is the charge-transfer resistance, A is the frequency factor, Ea is the apparent activation energy, R is the gas constant, and T is the absolute temperature.

Which was used to construct the Arrhenius plots. Ea values obtained this way are therefore apparent activation energies, but the relative trend across concentrations remains valid for mechanistic interpretation, as commonly practiced in EIS-based corrosion studies [82].

Where $1/R_{ct}$ was used as a surrogate for the apparent electrochemical kinetic parameter rather than as an exact corrosion rate, consistent with common practice in EIS-based corrosion studies. The resulting plot of $\ln(1/R_{ct})$ versus 1/T Fig. 15 gave excellent straight-line fits for all four systems R^2 = 0.9987-0.9999 from which the

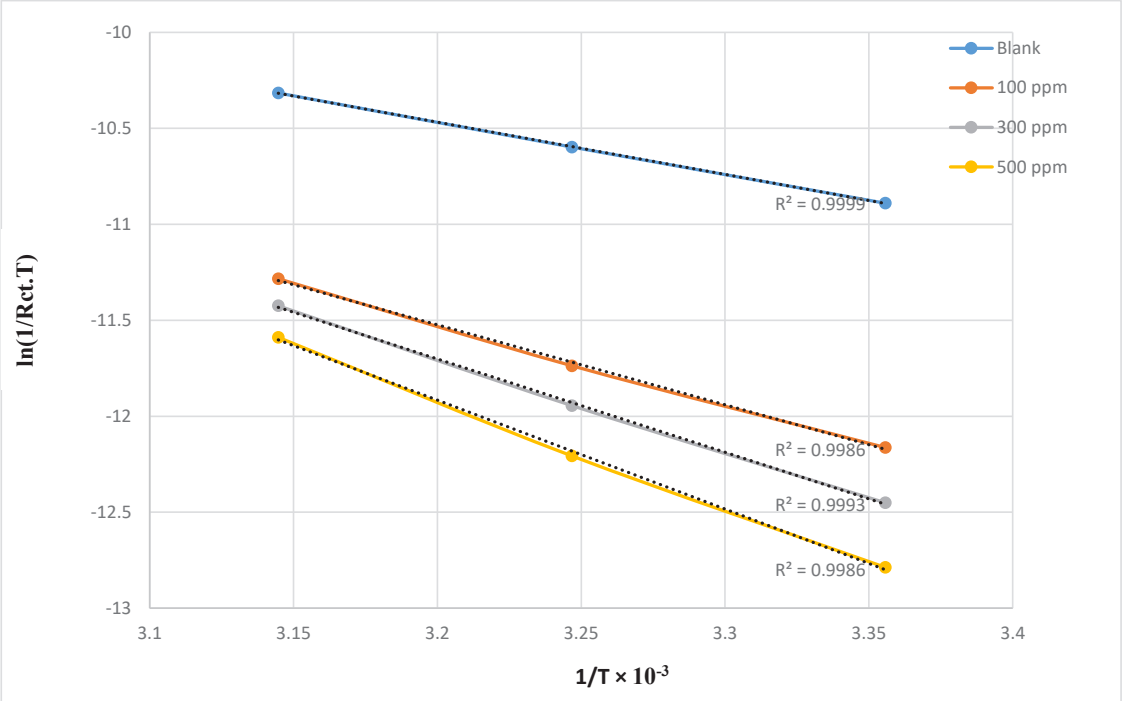

Fig. 18. Eyring plot [$\ln 1/R_{ct}.T$] versus 1/T for carbon steel corrosion in the blank and inhibited solution at different concentrations (100, 300, and 500 ppm)

Table 8. Apparent activation enthalpy ΔH* and apparent activation entropy ΔS* for carbon steel dissolution

System	ΔH* (KJ/mol)	ΔS* (J/mol.K)	R^2
Blank	22.6	-212.2	0.9999
100 ppm	34.6	-182.6	0.9986
300 ppm	40.4	-165.5	0.9993
500 ppm	47.2	-145.7	0.9986

apparent activation energies were extracted from the slope [83].

As shown in Table 7, the apparent activation energy Ea increased steadily with inhibitor concentration, from 25.2 KJ/mol in the blank solution to 49.7 KJ/mol at 500 ppm. An increase in the apparent activation energy Ea upon inhibitor addition suggests that the inhibitor increases the apparent energy barrier for the electrochemical process, most likely because adsorption progressively block active surface sites [84,85]. Although the apparent activation energy values are consistent with adsorption involving predominantly physical interactions, the Ea values alone cannot be considered conclusive evidence for distinguishing between physisorption and chemisorption [86].

Activation Thermodynamics (Eyring Analysis)

The Eyring transition-state equation was applied to complement the Arrhenius treatment:

$$Ln(1/R_{ct}.T) = [ln(R/Nh) + \Delta S/R] - \Delta H/RT$$

Plots of $ln(1/R_{ct}.T)$ versus 1/T were linear ($R^2 > 0.998$) for all systems Fig. 18, yielding ΔH* and ΔS* from the slop and intercept, respectively [87] (Table 8).

The apparent activation enthalpy ΔH* increased with inhibitor concentration following the general tread as the apparent activation energy Ea

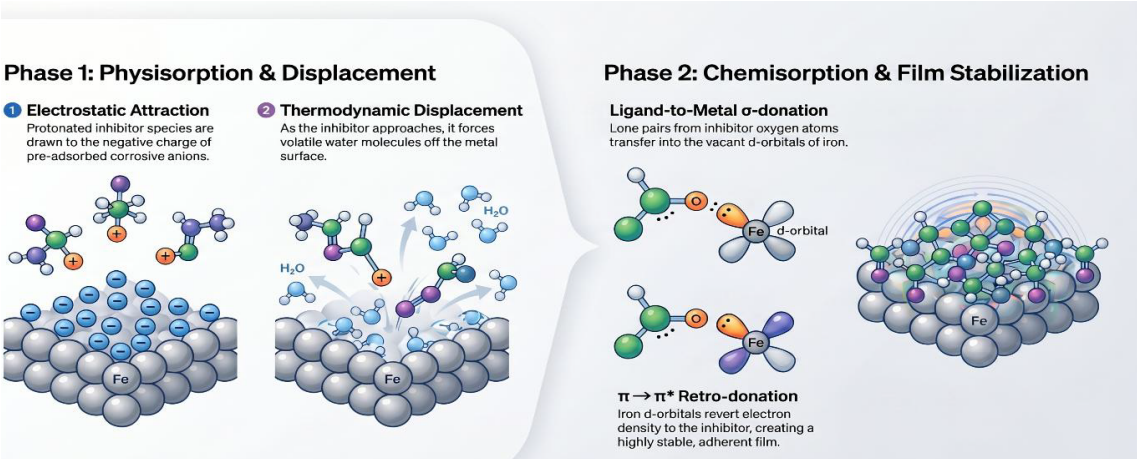

Fig. 19. Proposed dual-phase adsorption mechanism of AgNPs.Cin inhibitor on C45 steel surface

Table 9. Qualitative comparison of the present AgNPs.Cin inhibition with previously reported plant-based silver nanoparticle corrosion inhibitor in 1 M of HCl medium

SN	Plant Name	Plant part	Nano particle	Med.	Alloy used	Max %IE	Ref.
1	*Cinnamomum verum*	Bark	AgNPs.Cin	1 M HCl	Carbon steel	94 at 500 ppm, 298K (PDP) 85 at 500 ppm, 298K (EIS)	Current study
2	*Allium cepa*	Peels	AgNPs	1 M HCl	Carbon Steel	91.9 at 500 mg/L (PDP & EIS)	[91]
3	*Tobacco*	leaves	AgNPs	1 M HCl	carbon steel	95.3 at 200 ppm and 303K (PDP & EIS)	[92]
4	*cordia dichotoma extract*	leaves	AgNPs	1 M HCl	Mild steel	94.93 PDP at 400 ppm 87.33 EIS at 400 ppm	[93]
5	*Cryptocarya nigra* extract	leaves	AgNPs	1 M HCl	Mild steel	82.64 PDP at 500 ppm 91.05 EIS at 500 ppm	[94]

consistent with the relation Ea ≈ ΔH* + RT [88]. The more diagnostic result here is ΔS* its large negative values indicate that the activated complex is more ordered than the ground-state reactants, meaning the rate-determining step proceeds via an associative rather than a dissociative pathway consistent with formation of a compact Fe-H_2O/Cl^- transition complex at the metal surface [89]. As the concentration increased, the apparent activation entropy ΔS* become progressively less negative, suggesting that the adsorbed inhibitor raises the enthalpic barrier to this step without imposing additional conformational restriction on the transition complex itself. These observations suggest that the inhibitor primarily increase the apparent energy barrier of the electrochemical process rather than acting as a structural constraint on the activated state [90].

Comparative of the Present Green Inhibitor with Previously Published Eco-Friendly Inhibitors

To place the present findings in context, the performance of the proposed inhibitor was qualitatively compared with previously reported plant-based silver nanoparticle corrosion inhibitors. Because the published studies were conducted under different experimental conditions, including inhibitor concentration, temperature, steel type, and testing methodology, the comparison is intended only to provide a general qualitative perspective rather than a direct ranking of inhibition performance. The relevant studies are summarized in Table 9.

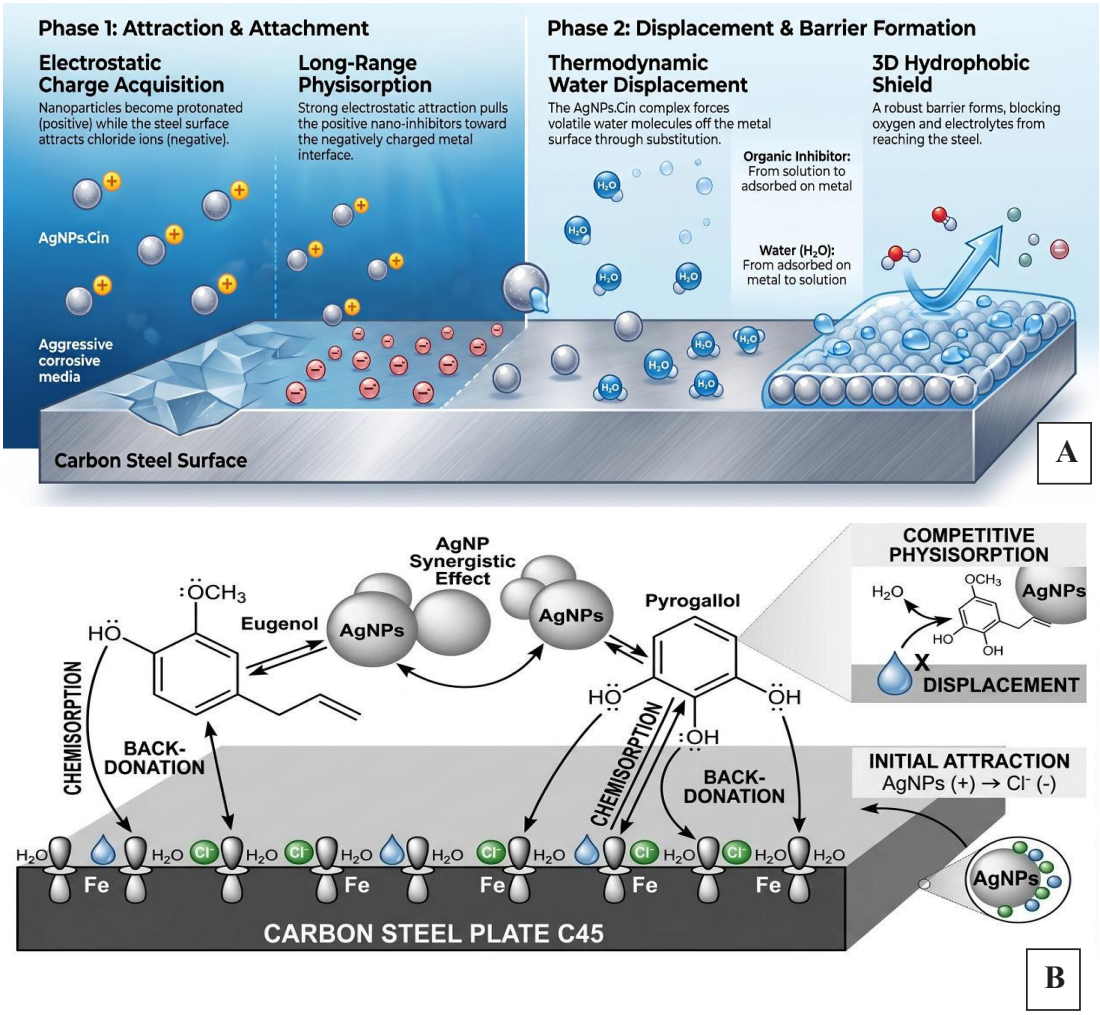

Fig. 20. The suggested adsorption mechanism of AgNPs.Cin

The suggested adsorption mechanism

Although the formulated green inhibitor comprises a complex mixture of diverse phytochemicals, its efficiency on the C45 carbon steel surface is primarily governed by the synergistic action between the biogenic silver nanoparticles AgNPs.Cin and the capping organic constituents (mainly Eugenol and Pyrogallol) [95]. The synthesized AgNPs.Cin nano complex features an abundance of heteroatoms (such as oxygen) with high electronegativity, alongside dense π-electron clouds residing within the aromatic ring and conjugated double bonds, include aldehydes, alcohols, esters, acids, monoterpenes, diterpenes, sesqui terpenes, benzopyrenes, hydrocarbons, phenolic compounds (Eugenol and pyrogallol), favonoids (procya nidin dimers type A and B), and phenolic compounds. Based on the combined electrochemical measurement (potentiodynamic polarization and electrochemical impedance spectroscopy), adsorption isotherm analysis, and the calculated thermodynamic and kinetic parameters, a plausible adsorption mechanism is proposed. The protective adsorbed layer illustrated in Fig. 19 is therefore inferred from this complementary result rather than directly confirmed by post-immersion surface characterization. The proposed inhibition process can be described through two distinct yet interconnected adsorption pathways [96-99].

Physisorption and Synergistic Molecular Displacement

Prior to chemical bonding, preliminary physical adsorption takes place via electrostatic interactions, In aggressive acidic or saline mediums, In aggressive acidic or chloride-containing environments, chloride ions (Cl^-) are specifically adsorbed onto the carbon steel surface, forming an anion-rich interfacial layer that promotes the subsequent adsorption of positively charged inhibitor species [100]. Concurrently, the heteroatoms of the AgNPs.Cin complex or the nanoparticle core itself can undergo protonation, acquiring a net positive charge. This induces a long-range electrostatic attraction (physisorption) between the protonated nano-inhibitor species and the Cl^--conditioned steel surface [101] As the AgNPs.Cin complex approaches the interface, it drives a thermodynamic displacement process, thermodynamically displaces the weakly adsorbed water molecules occupying the active sites, according to the substitution equilibrium [102]:

$$Org_{(sol)} + xH_2O_{(ads)} \rightleftharpoons Org_{(ads)} + xH_2O_{(sol)}$$

The replacement of interfacial water molecules by inhibitor species is expected to increases the surface coverage and enables. A more compact arrangement of the hydrophobic phytochemical constituents surrounding the AgNPs.Cin core [103]. This cooperative molecular packing is proposed to promote the development of an adsorbed hydrophobic barrier, which may reduce the transport of dissolved oxygen, chloride ions, and other aggressive electrolyte species toward the active corrosion sites, thereby contributing to lower anodic metal dissolution and cathodic reduction reactions [104]. Fig. 20a.

Chemisorption via Coordinate and Back-Donation Bonding

This pathway may involve the direct chemical interaction between the frontier orbitals of the inhibitor molecules and the steel substrate, as tentatively proposed in Fig. 20b. The lone pairs of electrons on the oxygen atoms of the hydroxyl (-OH) and methoxy ($-OCH_3$) groups may interact with the surface Fe atoms through coordinate bonding. Likewise, the π-electrons of the aromatic rings and the propene chain ($-CH=CH-CH_3$) may contribute to the adsorption process through possible π interactions with the metal surface. However, these interactions are tentatively proposed and were not directly confirmed in the present study [105]. A possible metal-to-ligand back-donation ($\pi \rightarrow \pi^*$ retro-donation) interaction has been proposed in the literature for similar inhibitor systems. However, such an interaction cannot be confirmed from the present experimental data because no surface spectroscopic or theoretical investigations were performed.

If such electronic interactions occur, they could contribute to the chemisorption of the mixed adsorption mechanism, complementing the initial physisorption process and enhancing the stability of the adsorbed inhibitor species on the steel surface [106]. Although this adsorption model is consistent with the electrochemical measurements, adsorption isotherm analysis, and the calculated thermodynamic, and kinetic parameters, the proposed molecular interactions remain hypothetical and cannot be directly confirmed because no surface spectroscopic

characterization (e.g., XPS) or theoretical calculations were performed in the present study.

Study limitation

The present study was designed to evaluate the corrosion inhibition performance of the final biosynthesized AgNPs.Cin nanocomposite. Therefore, the electrochemical experiments were performed by comparing the blank solution with the final inhibitor formulation. The individual contributions of cinnamon extract and silver nanoparticles were not investigated separately. Such control experiments would provide further insight into the specific role of each component and will be considered in future studies. In addition long-term corrosion performance was beyond the scope of the present study and will be investigated in future work. Furthermore, DLS and zeta-potential measurement were not performed, representing a limitation in assessing the colloidal stability of the AgNPs.Cin suspension and its effect on corrosion inhibition.

CONCLUSION

A green nano-inhibitor AgNPs.Cin was successfully synthesized using *Cinnamomum verum* extract. FESEM and TEM analyses confirmed the formation of predominantly spherical to semi-spherical nanoparticles, while EDX analysis verified the presence of silver. Electrochemical measurements (PDP and EIS) demonstrated that AgNPs.Cin effectively inhibited the corrosion of C45 carbon steel in 1.0 M HCl solution, with inhibition efficiency increasing as the inhibitor concentration increased and decreasing with increasing temperature. The adsorption behavior followed the Langmuir adsorption isotherm, whereas adsorption behavior followed the Langmuir adsorption isotherm, where the thermodynamic and kinetic analyses were consistent with a spontaneous adsorption process involving both physisorption and chemisorption. Overall, the green-synthesized AgNPs.Cin demonstrated promising potential as an environmentally friendly nano-inhibitor for the protection of C45 carbon steel in acidic media.

CONFLICT OF INTEREST

The authors declare that there is no conflict of interests regarding the publication of this manuscript.

REFERENCES

1. Al-Mhyawi SR. Green synthesis of silver nanoparticles and their inhibitory efficacy on corrosion of carbon steel in hydrochloric acid solution. International Journal of Electrochemical Science. 2023;18(9):100210.
2. Verma N, Kumar T, Vashistha VK, Das DK, Yadav S, Pullabhotla RVSR, et al. Anticorrosion properties of flavonoids for rust-free building materials: a review. Corros Rev. 2024;43(1):1-22.
3. Rashid KH, Khadom AA. Mathematical Modeling and Electrochemical Behavior for Corrosion Inhibition of Steel by Kiwi Juice Extract. Journal of Bio- and Tribo-Corrosion. 2019;6(1).
4. Farag AA, Elmesallamy SM, Bakry A, Fathy DS, El-Etre MA, Badr MM. One-pot synthesis of polybenzoxazine resin in situ blended with nano extract Lawsonia inermis as a shield coating for C-Steel in acidic environment: Experimental and theoretical approaches. Industrial Crops and Products. 2025;223:120306.
5. Ghanbari Daryaee S, Khormali A, Taleghani A, Mokaber-Esfahani M. Synergistic Effects of Rosemary and Carrot Extracts as Green Corrosion Inhibitors for Carbon Steel Protection in Acidizing Operations of Petroleum Industry. ChemEngineering. 2025;9(6):142.
6. Lubis HF, Natarisya H. Changes in the corrosion rate and microstructure of beta titanium wire using kiwi peel extract. Dental Journal (Majalah Kedokteran Gigi). 2023;56(2):122-126.
7. Kumar KS, Kathireswari P. Biological synthesis of Silver nanoparticles (Ag-NPS) by Lawsonia inermis (Henna) plant aqueous extract and its antimicrobial activity against human pathogens. International Journal of Current Microbiology and Applied Sciences. 2016;5(3):926-937.
8. Singh A, Ebenso EE, Quraishi MA. Corrosion Inhibition of Carbon Steel in HCl Solution by Some Plant Extracts. International Journal of Corrosion. 2012;2012:1-20.
9. Rukaiyat MS, Abubakar GS, Fatima MK. Corrosion inhibition of mild steel using alkaloids and tannins extracts of Jatropha curcas in acidic media. Bayero Journal of Pure and Applied Sciences. 2018;10(1):311.
10. Swathy O, Priya SS, Navada MK, Mulky L. Advances in corrosion inhibition: nanomaterials as sustainable solutions for protecting metals. Journal of Chemical Technology and Biotechnology. 2025;100(10):2004-2018.

11. Singh P, Singh A, Quraishi MA, Ebenso EE. Cetirizine: A New and Effective Corrosion Inhibitor for Mild Steel in 1 M HCl solution. International Journal of Electrochemical Science. 2012;7(8):7065-7079.
12. Al-Snafi AE. A REVIEW ON LAWSONIA INERMIS: A POTENTIAL MEDICINAL PLANT. International Journal of Current Pharmaceutical Research. 2019:1-13.
13. Al-aqbi ZT, Abdulsahib HT, Al-Doghachi FAJ. A Portable Microfluidic Device-Based Colorimetric Naked-Eye Sensors for Determination of Mercury and Arsenic Ions in River Water Samples. Plasmonics. 2024;19(6):3393-3414.
14. Singh H, Desimone MF, Pandya S, Jasani S, George N, Adnan M, et al. Revisiting the Green Synthesis of Nanoparticles: Uncovering Influences of Plant Extracts as Reducing Agents for Enhanced Synthesis Efficiency and Its Biomedical Applications. International Journal of Nanomedicine. 2023;Volume 18:4727-4750.
15. Md Ishak NAI, Kamarudin SK, Timmiati SN. Green synthesis of metal and metal oxide nanoparticles via plant extracts: an overview. Materials Research Express. 2019;6(11):112004.
16. Chen P, Sun J, Ford P. Differentiation of the Four Major Species of Cinnamons (C. burmannii, C. verum, C. cassia, and C. loureiroi) Using a Flow Injection Mass Spectrometric (FIMS) Fingerprinting Method. Journal of Agricultural and Food Chemistry. 2014;62(12):2516-2521.
17. Suresh D, Shobharani RM, Nethravathi PC, Pavan Kumar MA, Nagabhushana H, Sharma SC. Artocarpus gomezianus aided green synthesis of ZnO nanoparticles: Luminescence, photocatalytic and antioxidant properties. Spectrochimica Acta Part A: Molecular and Biomolecular Spectroscopy. 2015;141:128-134.
18. Al-Aqbi ZT, Albishri A, Hussein FH, Albukhaty S, Sulaiman GM, Khalil KAA, et al. A new 3D printing milli-fluidic device with integrated nanojunction for on-site colorimetric analysis of iron in water and soil samples. Chinese Journal of Analytical Chemistry. 2025;53(1):100475.
19. Premkumar J, Sudhakar T, Dhakal A, Shrestha JB, Krishnakumar S, Balashanmugam P. Synthesis of silver nanoparticles (AgNPs) from cinnamon against bacterial pathogens. Biocatalysis and Agricultural Biotechnology. 2018;15:311-316.
20. Elmitwalli O, Kassim DAK, Algahiny A, Henari F. Green Synthesis of Metal Nanoparticles Using Cinnamomum-Based Extracts and Their Applications. Nanotechnology, Science and Applications. 2025;Volume 18:93-114.
21. Pathak R, Sharma H. A Review on Medicinal Uses of Cinnamomum verum (Cinnamon). Journal of Drug Delivery and Therapeutics. 2021;11(6-S):161-166.
22. Albishri A, Al-aqbi ZT, Moker MH, Jebur NQ, Murad DMA. 3D Printed Microfluidic Device-Based Highly Sensitive and Selective Sensor for Detection of Human Albumin in Urine Samples. BioNanoScience. 2025;15(4).
23. Goutam SP, Saxena G, Singh V, Yadav AK, Bharagava RN, Thapa KB. Green synthesis of TiO2 nanoparticles using leaf extract of Jatropha curcas L. for photocatalytic degradation of tannery wastewater. Chem Eng J. 2018;336:386-396.
24. González-Anota DE, Paredes-Carrera SP, Pérez-Gutierrez RM, Arciniega-Caballero B, Borja-Urby R, Sánchez-Ochoa JC, et al. Green Synthesis by Microwave Irradiation of TiO2 Using Cinnamomum verum and the Application in Photocatalysis. Journal of Chemistry. 2023;2023:1-17.
25. Keshavarzi M, Najafi G, Ahmadi Gavlighi H, Seyfi P, Ghomi H. Enhancement of polyphenolic content extraction rate with maximal antioxidant activity from green tea leaves by cold plasma. J Food Sci. 2020;85(10):3415-3422.
26. Verma C, Ebenso EE, Quraishi MA. Ionic Liquids as Green Corrosion Inhibitors for Industrial Metals and Alloys. Green Chemistry: InTech; 2018. http://dx.doi.org/10.5772/intechopen.70421
27. Alaziz BA, Al-Shakban M, Al-aqbi ZT. Nanosensors-based integrated microfluidic devices for therapeutic drug monitorIng of fentanyl citrate, tramadol, and pethidine in blood plasma. Microfluid Nanofluid. 2025;29(12).
28. Usman I, Saputri AD, Arsyad WS, Ramadhan LOAN, Aba L, Hidayat R, et al. Green synthesizes of Silver Nanoparticles (AgNP) from Henna Leaf Extract (Lawsonia Inermis) and Its Chemical and Physical Properties as Photo-sensitizers in The DSSC. Journal of Physics: Conference Series. 2025;2980(1):012001.
29. Shamnamol GK, John S, Jacob JM. Exploring the Corrosion Inhibition Efficacy of Epoxy Merged Silver Nanoparticle Synthesized Using Garcinia gummi-gutta Leaf Extract Against Mild

Steel in an Acidic Medium. Journal of Bio- and Tribo-Corrosion. 2023;9(4).
30. Obaid NAM, Faisal NH, Ali NW, Ibrahim RG, Hassan AN, Kadhum AJ, et al. Synthesis, characterization, and biological activity of silver nanofibers essential oils of prunus dulcis. Egyptian Pharmaceutical Journal. 2024.
31. Khudhair NA, Al-Sammarraie AMA. Role of Carbon Dioxide on the Corrosion of Carbon Steel Reinforcing Bar in Simulating Concrete Electrolyte. Baghdad Science Journal. 2020;17(1).
32. Khudhair NA, Al-Sammarraie AMA. Enhancing of Corrosion Protection of Steel Rebar in Concrete Using TiO2 Nanoparticles as Additive. Iraqi Journal of Science. 2019:1898-1903.
33. Antifungal activity of silver nanoparticles green biosynthesis from the extract of Zygophyllum album (L.f.) on Fusarium wilt. Journal of Plant Protection Research. 2023.
34. Faisal N, Obaid N, Ali N, Al-Shawi A, Ibrahim R, Hassan A, et al. Green Synthesis of Silver Nanoparticles Using the Seeds of Lupinus luteus: Characterization and Assessment the Antibacterial and Anticancer Activities. Asian Pac J Cancer Prev. 2025;26(9):3405-3414.
35. Vijayan R, Joseph S, Mathew B. Eco-friendly synthesis of silver and gold nanoparticles with enhanced antimicrobial, antioxidant, and catalytic activities. IET Nanobiotechnology. 2018;12(6):850-856.
36. Panasiewicz K. Chemical Composition of Lupin (Lupinus spp.) as Influenced by Variety and Tillage System. Agriculture. 2022;12(2):263.
37. Laxman SV, Srinivas Y, Anita RD, Jayadev NH, Channayya IS, Somlingesh NS. Antimicrobial activity of the biosynthesized silver nanoparticles of Gossypium hirsutum leaves extract. GSC Biological and Pharmaceutical Sciences. 2021;15(3):189-198.
38. Ahmad A, Mushtaq Z, Saeed F, Afzaal M, Al Jbawi E. Ultrasonic-assisted green synthesis of silver nanoparticles through cinnamon extract: biochemical, structural, and antimicrobial properties. Int J Food Prop. 2023;26(1):1984-1994.
39. Aravind M, Kumaresubitha T, Ahmed N, Velusamy P. DFT, molecular docking, photocatalytic and antimicrobial activity of coumarin enriched Cinnamon bark extract mediated silver nanoparticles. Inorg Chem Commun. 2022;146:110176.
40. Vishwajeet S, Ankita S, Nitin W. Biosynthesis of silver nanoparticles by plants crude extracts and their characterization using UV, XRD, TEM and EDX. African Journal of Biotechnology. 2015;14(33):2554-2567.
41. Das R, kumar u. Exploring the anti-convulsant potential of cordia dichotoma leaf extract to combat seizures in swiss albino mice. Springer Science and Business Media LLC; 2025. http://dx.doi.org/10.21203/rs.3.rs-8395823/v1
42. Singh J, Dutta T, Kim K-H, Rawat M, Samddar P, Kumar P. 'Green' synthesis of metals and their oxide nanoparticles: applications for environmental remediation. Journal of Nanobiotechnology. 2018;16(1).
43. Grela ER, Kiczorowska B, Samolińska W, Matras J, Kiczorowski P, Rybiński W, et al. Chemical composition of leguminous seeds: part I—content of basic nutrients, amino acids, phytochemical compounds, and antioxidant activity. European Food Research and Technology. 2017;243(8):1385-1395.
44. Alharbi NS, Alsubhi NS, Felimban AI. Green synthesis of silver nanoparticles using medicinal plants: Characterization and application. Journal of Radiation Research and Applied Sciences. 2022;15(3):109-124.
45. Swapna G, Rao BK. Green Synthesis and Characterization of Silver Nanoparticles from Stem Bark Extract of Cordia dichotoma G. Forst and Evaluation of their Antioxidant and Antibacterial activities Articles. Pharmacognosy Res. 2021;13(3):158-164.
46. Loganathan S, Selvam K, Shivakumar MS, Senthil-Nathan S, Vasantha-Srinivasan P, Gnana Prakash D, et al. Phytosynthesis of Silver Nanoparticle (AgNPs) Using Aqueous Leaf Extract of Knoxia sumatrensis (Retz.) DC. and Their Multi-Potent Biological Activity: An Eco-Friendly Approach. Molecules. 2022;27(22):7854.
47. Rudrappa M, Rudayni HA, Assiri RA, Bepari A, Basavarajappa DS, Nagaraja SK, et al. Plumeria alba-Mediated Green Synthesis of Silver Nanoparticles Exhibits Antimicrobial Effect and Anti-Oncogenic Activity against Glioblastoma U118 MG Cancer Cell Line. Nanomaterials. 2022;12(3):493.
48. Nemattalab M, Rohani M, Evazalipour M, Hesari Z. Formulation of Cinnamon (Cinnamomum verum) oil loaded solid lipid nanoparticles and evaluation of its antibacterial activity against

Multi-drug Resistant Escherichia coli. BMC Complementary Medicine and Therapies. 2022;22(1).
49. Zhou J, Zheng X, Cai Q, Song C. Introducing a Novel Chemotherapeutic Drug for the Treatment of Lung Adenocarcinoma: Silver Nanoparticles Green-formulated by Cinnamomum verum. Journal of Oleo Science. 2022;71(3):371-378.
50. Electrochemical analysis of corrosion process of steel bar in fluid simulating porous concrete. Functional Materials. 2020;27(4).
51. Abdel-Hameed R, Qureshi MT, Abdallah M, Aljuhani E, Alzharani AA, Alfarsi A, et al. Recycling of Expired Lactulose Drugs as Eco-Friendly Corrosion Inhibitor for Steel Alloys in Acidic Environment: Gravimetrical and Electrochemical Studies. International Journal of Electrochemical Science. 2022;17(12):221270.
52. Verma C, Quraishi MA, Kluza K, Makowska-Janusik M, Olasunkanmi LO, Ebenso EE. Corrosion inhibition of mild steel in 1M HCl by D-glucose derivatives of dihydropyrido [2,3-d:6,5-d'] dipyrimidine-2, 4, 6, 8(1H,3H, 5H,7H)-tetraone. Sci Rep. 2017;7(1).
53. El-Sayed A-R, El-Hendawy MM, El-Mahdy MS, Hassan FSM, Mohamed AE. The inhibitive action of 2-mercaptobenzothiazole on the porosity of corrosion film formed on aluminum and aluminum–titanium alloys in hydrochloric acid solution. Sci Rep. 2023;13(1).
54. Deng S, Li X, Fu H. Acid violet 6B as a novel corrosion inhibitor for cold rolled steel in hydrochloric acid solution. Corros Sci. 2011;53(2):760-768.
55. Li X, Deng S, Fu H. Triazolyl blue tetrazolium bromide as a novel corrosion inhibitor for steel in HCl and H2SO4 solutions. Corros Sci. 2011;53(1):302-309.
56. Ibrahim MM, Abdel Hameed RS, Abu-Nawwas AAH, Mohamad SE. ChemInform Abstract: Schiff's Bases and Their Metal Complexes as Corrosion Inhibitors for Aluminum Alloys in Corrosive Media. ChemInform. 2016;47(21).
57. Asafa TB, Odusote JK, Ibrahim OS, Lateef A, Durowoju MO, Azeez MA, et al. Inhibition efficiency of silver nanoparticles solution on corrosion of mild steel, stainless steel and aluminum in 1.0 M HCl medium. IOP Conference Series: Materials Science and Engineering. 2020;805(1):012018.
58. Abdel Hameed RS. Schiff' Bases as Corrosion Inhibitor for Aluminum Alloy in Hydrochloric Acid Medium. Tenside Surfactants Detergents. 2019;56(3):209-215.
59. Corrosion Inhibitor for Mild Steel in Mixed HCl and H_2SO_4 Medium: A Study of 1,10-Phenanthroline Derivatives. American Chemical Society (ACS). http://dx.doi.org/10.1021/acsomega.5c01412.s001
60. Sharma V, Borse M, Jauhari S, Pai KB, Devi S. New Hydroxylated Cationic Gemini Surfactants as Effective Corrosion Inhibitors for Mild Steel in Hydrochloric Acid Medium. Tenside Surfactants Detergents. 2005;42(3):163-167.
61. Abdel Hameed RS, Al-bonayan AM. Recycling of Some Water Soluble Drugs for Corrosion Inhibition of Steel Materials: Analytical and Electrochemical Measurements. Journal of Optoelectronic and Biomedical Materials. 2021;13(2):45-55.
62. Al-Sabagh AM, Kandil NG, Ramadan O, Amer NM, Mansour R, Khamis EA. Novel cationic surfactants from fatty acids and their corrosion inhibition efficiency for carbon steel pipelines in 1M HCl. Egyptian Journal of Petroleum. 2011;20(2):47-57.
63. Noor EA. Temperature Effects on the Corrosion Inhibition of Mild Steel in Acidic Solutions by Aqueous Extract of Fenugreek Leaves. International Journal of Electrochemical Science. 2007;2(12):996-1017.
64. A new synthesized coumarin-derived Schiff base as a corrosion inhibitor of mild steel surface in HCl medium: gravimetric and DFT studies. International Journal of Corrosion and Scale Inhibition. 2020;9(1).
65. Kokalj A. On the use of the Langmuir and other adsorption isotherms in corrosion inhibition. Corros Sci. 2023;217:111112.
66. Umoren SA, Banera MJ, Alonso-Garcia T, Gervasi CA, Mirífico MV. Inhibition of mild steel corrosion in HCl solution using chitosan. Cellulose. 2013;20(5):2529-2545.
67. Application of expired Co-amoxiclav medicinal drugs for corrosion inhibition of steel alloys used in petroleum industry in acidic environment. International Journal of Corrosion and Scale Inhibition. 2021;10(2).
68. Effect of organic corrosion inhibitors functional groups (azo and azomethine) on carbon steel N80 alloy corrosion using the electrochemical polarization technique. International Journal of Corrosion and Scale Inhibition. 2024;13(1).
69. Hameed RSA. Ranitidine Drugs as Non-

Toxic Corrosion Inhibitors for Mild Steel in Hydrochloric Acid Medium. Portugaliae Electrochimica Acta. 2011;29(4):273-285.
70. Abdel Hameed RS, Aleid GMS, Mohammad D, Badr MM, Huwaimel B, Sh. Suliman M, et al. Spinacia oleracea Extract as Green Corrosion Inhibitor for Carbon Steel in Hydrochloric Acid Solution. International Journal of Electrochemical Science. 2022;17(10):221017.
71. Şahin EA, Solmaz R, Gecibesler İH, Kardaş G. Adsorption ability, stability and corrosion inhibition mechanism of phoenix dactylifera extrat on mild steel. Materials Research Express. 2020;7(1):016585.
72. Belkhaouda M, Bammou L, Salghi R, Zarrouk A, Ebenso EE, Zarrok H, et al. Inedible Avocado Extract: An Efficient Inhibitor of Carbon Steel Corrosion in Hydrochloric Acid. International Journal of Electrochemical Science. 2013;8(9):10987-10999.
73. Aslam R, Mobin M, Shoeb M, Aslam J. Novel ZrO_2-glycine nanocomposite as eco-friendly high temperature corrosion inhibitor for mild steel in hydrochloric acid solution. Sci Rep. 2022;12(1).
74. Essien EA, Kavaz D, Ituen EB, Umoren SA. Synthesis, characterization and anticorrosion property of olive leaves extract-titanium nanoparticles composite. J Adhes Sci Technol. 2018;32(16):1773-1794.
75. Lagrenée M, Mernari B, Bouanis M, Traisnel M, Bentiss F. Study of the mechanism and inhibiting efficiency of 3,5-bis(4-methylthiophenyl)-4H-1,2,4-triazole on mild steel corrosion in acidic media. Corros Sci. 2002;44(3):573-588.
76. Shahmoradi AR, Talebibahmanbigloo N, Javidparvar AA, Bahlakeh G, Ramezanzadeh B. Studying the adsorption/inhibition impact of the cellulose and lignin compounds extracted from agricultural waste on the mild steel corrosion in HCl solution. J Mol Liq. 2020;304:112751.
77. Shahmoradi AR, Ranjbarghanei M, Javidparvar AA, Guo L, Berdimurodov E, Ramezanzadeh B. Theoretical and surface/electrochemical investigations of walnut fruit green husk extract as effective inhibitor for mild-steel corrosion in 1M HCl electrolyte. J Mol Liq. 2021;338:116550.
78. Elmi F, Valipour E, Ghasemi S. Synthesis of anticorrosion nanohybrid films based on bioinspired dopamine, L-cys/CNT@PDA through self-assembly on 304 stainless steel in 3.5% NaCl. Bioelectrochemistry. 2019;126:79-85.
79. Mansfeld F, Shih H, Greene H, Tsai CH. Analysis of EIS Data for Common Corrosion Processes. Electrochemical Impedance: Analysis and Interpretation: ASTM International100 Barr Harbor Drive, PO Box C700, West Conshohocken, PA 19428-2959; 1993. p. 37-53. http://dx.doi.org/10.1520/stp18062s
80. Emran KM, Ouerfelli N. Effect of acid proticity on the thermodynamic parameters of charge transfer resistance in corrosion and passivation of nickel based glass alloy. Sci Rep. 2024;14(1).
81. Emran KM, Omar IMA, Arab ST, Ouerfelli N. On the pseudo-hyperbolic behavior of charge transfer resistance–temperature dependence in corrosion behavior of Nickel based glass alloy. Sci Rep. 2022;12(1).
82. Adamu AA, Iyun ORA, Habila JD. Adsorption and thermodynamic studies of the corrosion Inhibition effect of Desmodium adscendens (Swartz) extract on carbon steel in 2 M HCl. BMC Chemistry. 2025;19(1).
83. Akinbulumo OA, Odejobi OJ, Odekanle EL. Thermodynamics and adsorption study of the corrosion inhibition of mild steel by Euphorbia heterophylla L. extract in 1.5 M HCl. Results in Materials. 2020;5:100074.
84. Zarrouk A, El Ouali I, Bouachrine M, Hammouti B, Ramli Y, Essassi EM, et al. Theoretical approach to the corrosion inhibition efficiency of some quinoxaline derivatives of steel in acid media using the DFT method. Res Chem Intermed. 2012;39(3):1125-1133.
85. Inhibition of mild steel corrosion in 0.5 M sulfuric acid by an aqueous extract of leaves of Tectona grandis L. plant. International Journal of Corrosion and Scale Inhibition. 2021;10(4).
86. Al-Amiery A, Isahak WNRW, Al-Azzawi WK. Multi-method evaluation of a 2-(1,3,4-thiadiazole-2-yl)pyrrolidine corrosion inhibitor for mild steel in HCl: combining gravimetric, electrochemical, and DFT approaches. Sci Rep. 2023;13(1).
87. Preethi Kumari P, Shetty P, Rao SA. Electrochemical measurements for the corrosion inhibition of mild steel in 1 M hydrochloric acid by using an aromatic hydrazide derivative. Arabian Journal of Chemistry. 2017;10(5):653-663.
88. Ikeuba AI, Ntibi JE, Okafor PC, Ita BI, Agobi AU, Asogwa FC, et al. Kinetic and thermodynamic evaluation of azithromycin as a green corrosion inhibitor during acid cleaning process of mild

steel using an experimental and theoretical approach. Results in Chemistry. 2023;5:100909.
89. Noor EA, Al-Moubaraki AH. Thermodynamic study of metal corrosion and inhibitor adsorption processes in mild steel/1-methyl-4[4′(-X)-styryl pyridinium iodides/hydrochloric acid systems. Materials Chemistry and Physics. 2008;110(1):145-154.
90. Elayyachy M, Hammouti B, Vercelli B, El-Idrissi A, Aouniti A. Adsorption and Corrosion Inhibition Behavior of C38 Steel by one Derivative of Quinoxaline in 1 M HCl. Portugaliae Electrochimica Acta. 2011;29(1):57-68.
91. Ituen E, Singh A, Yuanhua L, Akaranta O. Green synthesis and anticorrosion effect of Allium cepa peels extract-silver nanoparticles composite in simulated oilfield pickling solution. SN Applied Sciences. 2021;3(6).
92. The inhibition of the steel corrosion in hydrochloric acid solution by juice of Prunus cerasus. International Journal of Electrochemical Science. 2006.
93. Ibrahim RQ, Ali SH, Faisal NH, Ibrahim SQ, Al-Shawi AAA, Hassan AN, et al. Green synthesis of silver nanoparticles using Cordia dichotoma leaves and their application as a corrosion inhibitor of mild steel in 1.0 M HCl. International Journal of Corrosion and Scale Inhibition. 2026;15(2):253-271.
94. Faiz M, Zahari A, Awang K, Hussin H. Corrosion inhibition on mild steel in 1 M HCl solution by Cryptocarya nigra extracts and three of its constituents (alkaloids). RSC Advances. 2020;10(11):6547-6562.
95. Cinnamomum zeylanicum Bark Extract. Definitions: Qeios; 2020.
96. Souza VB, Holkem AT, Thomazini M, Petta T, Tulini FL, Oliveira CAF, et al. Study of extraction kinetics and characterization of proanthocyanidin-rich extract from Ceylon cinnamon (Cinnamomum zeylanicum). J Food Process Preserv. 2021;45(5).
97. Alotaibi WM, Al-Mhyawi SR, Albukhari SM. Chitosan-Clay Nanocomposite as a Green Corrosion Inhibitor for Mild Steel in Hydrochloric Acid Solution. International Journal of Electrochemical Science. 2022;17(8):220848.
98. Odusote JK, Ajayi OM. Corrosion Inhibition of Mild Steel in Acidic Medium by Jathropha Curcas Leaves Extract. Journal of Electrochemical Science and Technology. 2013;4(2):81-87.
99. Pourmohseni M, Rashidi A, Karimkhani M. Preparation of corrosion inhibitor from natural plant for mild stil immersed in an acidic environmental: experimental and theoretical study. Sci Rep. 2024;14(1).
100. Singh AK, Quraishi MA. The effect of some bis-thiadiazole derivatives on the corrosion of mild steel in hydrochloric acid. Corros Sci. 2010;52(4):1373-1385.
101. Ahmed MI, Abd-El-Raouf M, Migahed MA, Ibrahim MAM, Rizk SA, Basiony NME. Corrosion inhibition mechanism of a functionalized schiff base–derived quaternary ammonium salt for carbon steel in 1 M HCl: electrochemical, adsorption, and theoretical studies. Sci Rep. 2026;16(1).
102. Hmamou DB, Salghir R, Zarrouk A, Zarrok H, Al-Deyab SS, Benali O, et al. The Inhibited effect of Phenolphthalein towards the corrosion of C38 Steel in Hydrochloric Acid. International Journal of Electrochemical Science. 2012;7(9):8988-9003.
103. Ghareba S, Omanovic S. Interaction of 12-aminododecanoic acid with a carbon steel surface: Towards the development of 'green' corrosion inhibitors. Corros Sci. 2010;52(6):2104-2113.
104. Uhlig HH, Triadis DN, Stern M. Effect of Oxygen, Chlorides, and Calcium Ion on Corrosion Inhibition of Iron by Polyphosphates. J Electrochem Soc. 1955;102(2):59.
105. Solmaz R, Kardaş G, Çulha M, Yazıcı B, Erbil M. Investigation of adsorption and inhibitive effect of 2-mercaptothiazoline on corrosion of mild steel in hydrochloric acid media. Electrochimica Acta. 2008;53(20):5941-5952.
106. Abulyazid I, Mahdy EME, Ahmed RM. Biochemical study for the effect of henna (Lawsonia inermis) on Escherichia coli. Arabian Journal of Chemistry. 2013;6(3):265-273.